Electronic Thesis and Dissertation Repository

12-3-2012 12:00 AM

Nanomechanics of Electrospun Nanofibres for Tissue Engineering of the Tympanic Membrane

Sara Makaremi
The University of Western Ontario

Supervisor
Dr. Wankei Wan
The University of Western Ontario

Recommended Citation

NANOMECHANICS OF ELECTROSPUN NANOFIBRES FOR TISSUE ENGINEERING OF THE TYMPANIC MEMBRANE

(Spine title: Nanomechanics of Electrospun Fibres)

(Thesis format: Monograph)

by

Sara <u>Makaremi</u>

Graduate Program in Biomedical Engineering

A thesis submitted in partial fulfillment
of the requirements for the degree of
Master of Engineering Science

The School of Graduate and Postdoctoral Studies
The University of Western Ontario
London, Ontario, Canada

THE UNIVERSITY OF WESTERN ONTARIO
School of Graduate and Postdoctoral Studies

CERTIFICATE OF EXAMINATION

Supervisor	Examiners
_____	_____
Dr. Wankei Wan	Dr. Hanif Ladak
Supervisory Committee	_____
_____	Dr. Murad Husein
Dr. Jeffrey L. Hutter	_____
_____	Dr. Andrew Hrymak
Dr. Hanif Ladak	
_____	
Dr. Sumit Agrawal	

The thesis by

Sara <u>Makaremi</u>

entitled:

**Nanomechanics of Electrospun Nanofibres for Tissue Engineering of
the Tympanic Membrane**

is accepted in partial fulfilment of the
requirements for the degree of
Master of Engineering Science

Date_____   _____
                                            Chair of the Thesis Examination Board

Abstract

The Tympanic Membrane (TM), also known as the eardrum, includes layers of organized collagen nanofibres which play an essential role in sound transmission. Perforations that are caused by infection or accident must be repaired in order to restore hearing. Tympanoplasty is performed using grafts that are prepared from bladder, cartilage, temporal fascia and cadaveric skin. However, since mechanical properties of these grafts do not match those of the original TM, normal hearing is not fully restored. The goal of this study is to develop nanofibrous scaffolds for tissue engineering of the TM in order to circumvent the complications addressed with the conventional grafts. Mechanical properties of scaffolds greatly influence cellular behaviour, since cells can sense and respond to the stiffness of their substrate. In this study we investigated the Young's modulus of single poly(caprolactone) (PCL) nanofibres as well as the moduli of as-spun and genipin-cross-linked collagen type I nanofibres using multi-point bending test with atomic force microscope (AFM). The effect of shear and tension on bending behaviour of fibres was investigated using four different analytical models. The Young's modulus of electrospun PCL fibres ($100 < d < 400$ nm) was obtained with a mean value of 0.48 ± 0.03 GPa. For as-spun and genipin-cross-linked collagen nanofibres a range of $1.66 - 13.9$ GPa and $8.22 - 40.1$ GPa were found for their Young's moduli, respectively. The results indicate that there is a great potential for electrospun PCL and collagen nanofibres to be successfully applied in tissue engineering scaffolds because of their promising mechanical properties and biocompatibility.

Keywords*: Multi-Point Bending Test, Atomic Force Microscopy, Electrospinning, Poly(caprolactone) Nanofibres, Young's Modulus, Collagen Type I, Genipin Cross-linking, Tympanic Membrane, Tissue Engineering

Acknowledgements

First and foremost, I would like to sincerely thank my supervisors Dr. Wankei Wan and Dr. Jeffrey L. Hutter for their guidance and encouragement over the last two years. I would like to thank Dr. Wan in particular for providing me with the opportunity to study in the BME program at Western, and to have this invaluable learning experience in his research group. I would also like to thank Dr. James Johnson, the director of the BME program, for his invaluable suggestions and insightful questions during my seminar presentations.

Much of this work would not have been possible without the help and technical expertise of Dr. Hutter, particularly on mechanical testing with Atomic Force Microscope (AFM). I would like to thank him for spending his valuable time on training me with AFM, and explaining the theoretical concepts in detail. I greatly appreciate his continuous support and insightful suggestions. Dr. Hutter was always willing to discuss various aspects of my thesis and answered my numerous questions with enthusiasm and patience. He taught me that there is no such thing as failure in research and that any task can be accomplished if it is done one step at a time.

My gratitude also extends to my advisory committee: Dr. Hanif Ladak and Dr. Sumit Agrawal. I greatly appreciate their technical advice and their helpful suggestions. Also, I would like to thank Dr. Richard Gardiner, Nicole Bechard, and Karen Nygard from Biotron Facility for their assistance and technical expertise with SEM, TEM and confocal imaging. Particularly, I greatly appreciate Dr. Gardiner's insightful suggestions on imaging hollow fibres with TEM.

My past and present colleagues at the engineering and physics laboratory: Erica Lee, Ying (Betty) Li, Dr. Jian Liu, Asha Parekh, Marko Spaic, Justin Cook, Darcy Small, Dr. Karen Kennedy, Dr. Elaine Wong, Arian Gholami, Adam Golin, Dr. Stephen Hudson, Dr. Hadi Mahdavi, Dusa Vukosavljevic, Rafael Schulman, Himasha Medhavi Wijesekara, thank you all for your valuable friendship and your suggestions during weekly group meetings and presentation rehearsals.

Table of Contents

List of Figures

List of Tables

List of Appendices

Chapter 1: Introduction

The tympanic membrane (TM), also known as the eardrum, plays an essential role in sound transmission from the outer to the middle ear. Perforations that are caused by infections or accidental trauma need to be repaired in order to restore hearing, since normal hearing function strongly depends on the TM integrity. Although the TM has a self-healing mechanism that can repair small perforations spontaneously, the repaired tissue can be flawed in terms of its layer structure [1]. The middle fibrous layer in the TM has a special organization, with collagen fibres mostly oriented in radial and circumferential directions, which is critical for its acoustic characteristics [2]. Currently, tympanoplasty is performed by closure of the perforated TM with autologous grafts such as bladder [3], temporal fascia [4], or cartilage [5], or with commercial grafts prepared from cadaveric skin [6, 7]. However, since the mechanical and acoustic properties of these grafts do not match those of the original tissue, normal hearing is not fully restored [2]. Also, there is a risk of disease transmission when cadaveric or homologous skin grafts are used. The hypothesis is that these complications can be overcome if the traditional grafts are replaced by tissue engineered scaffolds.

Since cells can sense and respond to the stiffness of their substrate, the mechanical properties of scaffolds directly influence cellular activities within a tissue-engineered construct [8]. Therefore, in nanofibrous scaffolds it is essential to determine and tune the elastic modulus of single nanofibres to which cells anchor themselves. Moreover, the overall mechanical properties of a fibrous scaffold are a function of the mechanical properties of individual fibres and the orientation of the fibres within the scaffold [9]. In this study, we aim to determine the stiffness of single poly(caprolactone) and collagen nanofibres in order to verify their potential application as scaffold materials for tissue engineering of the TM.

Poly(caprolactone) (PCL) is a biocompatible and biodegradable polymer which has several FDA-approved biomedical applications such as medical sutures and drug delivery

devices [10]. PCL is considered as an attractive biomaterial since after degradation its by-products are neutral and do not change the pH of the natural environment [11]. Electrospinning has been utilized to create nonwoven nanofibrous PCL scaffolds for tissue engineering applications [12]. Scaffolds created using electrospinning show high surface area to volume ratio, high porosity, and high pore interconnectivity which are essential for cell adhesion, migration, and proliferation [13].

Collagen has been used in various tissue engineering applications and is considered as one of the most ideal biopolymers for fabrication of scaffolds since it is biocompatible, degradable, and has high water affinity [14]. Moreover, the abundance of collagen in the extra cellular matrix (ECM), and its unique mechanical properties make it a vital component in many tissue engineering applications. To date, several researchers have successfully developed fibrous scaffolds by electrospinning collagen [14].

Conventional macroscopic tensile testing is not suitable for measuring the elasticity of individual nanometer sized fibres. On the other hand, nanoindenter-based tensile tests which have been used to obtain elastic-plastic behaviour of single fibres [15], and micro-electromechanical systems used for tensile testing are both expensive and time consuming [16]. Moreover, other techniques such as the nano-tensile testing for electrospun fibres, require proper fibre gripping and fibre alignment [17].

The nanometer-scale lateral resolution of the Atomic Force Microscope (AFM) and its ability to measure subnanonewton forces have made it possible to investigate the mechanical properties of nanofibres [18]. Salvetat *et al.* (1999) first used the AFM for bending a suspended nanofibre using a three-point bending test in which a known force was applied at the midpoint of a fibre suspended over a gap [19]. Using a clamped beam model [20], the deflection of the fibre at the centre point was used to determine the elasticity of the fibre. In order to eliminate the uncertainty of precisely locating the centre of the fibre, a multipoint bending test was later introduced by Guhados *et al.* [21]. This method had the additional advantage of simultaneously allowing validation of the model applied. We have used the same approach for all mechanical characterization experiments

2

conducted in this study. Moreover, we have applied four different analytical models to analyze the data obtained from the bending experiments.

The main objective of this study is to determine the Young's modulus of single electrospun PCL and collagen nanofibres, using a multipoint bending test with AFM, to investigate their potential application for tissue engineering of the tympanic membrane.

Chapter 2: Background & Literature Review

2.1 Tympanic Membrane

2.1.1 Structure and Function

The Tympanic Membrane (TM), also known as the eardrum, separates the outer ear from the inner ear. The first and the most crucial step in the sound transmission process takes place at the TM. It transmits sound vibration from the air of the external ear canal to the fluid of the inner ear. The structure of the TM comprises a large, tightly-stretched tissue, and is termed Pars Tensa (Fig. 2.1). In contrast, Pars Flaccida is a small portion of the TM which is thicker and much more compliant, and contains vessels, nerve endings, and mast cells [22]. The Pars Tensa is a funnel-shaped membrane which has three layers: the epidermal layer, which is continuous with the mucosa of the middle ear; the lamina propria, which includes radial and circumferential collagen fibres; and the medial mucosal layer [23]. Knutsson *et al.* have investigated the distribution of different collagen types in the healthy human tympanic membrane [24]. They have reported that collagen Type II is the most abundant collagen in the lamina propria, particularly in the radial direction, and collagen Type III is mostly found in the circumferential fibres [24].
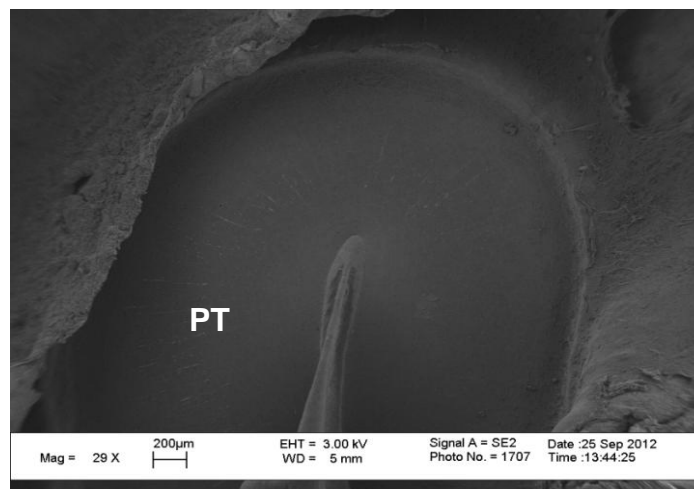
Fig. 2.1: Scanning Electron Microscope (SEM) image of the TM of rat, showing the Pars Tensa (PT) in TM (Courtesy of Dr. Jian Liu)

4

It is believed that fibre arrangement in the tympanic membrane leads to its unique acoustic and mechanical properties [2]. Several researchers have investigated the tympanic membrane of various animals to explain the relationship between the vibration pattern and the different layers in the TM [25, 22, 26]. However, to date, only a few studies have examined the arrangement of collagen fibres in lamina propria of the TM and its relation to its acoustic properties [2]. Kawabata *et al.* have reported their detailed observation of collagen fibres in the tympanic membrane of guinea pigs using scanning electron microscopy (SEM) [27]. They reported that radial and circumferentially oriented collagen fibres were found in the TM of guinea pigs. In a recent study, similar alignment was observed for the collagen fibres in the tympanic membrane of Wistar rats (Fig. 2.2).
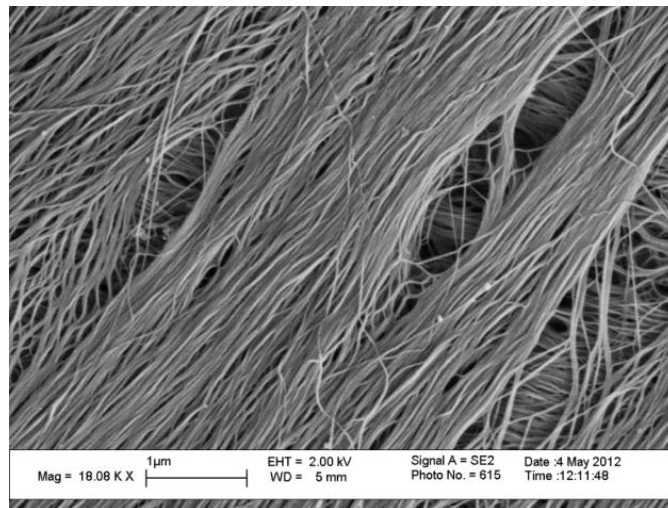
Fig. 2.2: SEM image of the TM from healthy adult Wistar rats, showing organized alignment of collagen fibres in two directions (Courtesy of Dr. Jian Liu)

2.1.2 TM Perforation & Treatment

Perforations of the eardrum are holes or ruptures that are caused by infections or trauma, such as skull fracture or high-level impulsive sound pressure as a result of an explosion. Among common infections, Acute Otitis Media (AOM) is a childhood infection that may cause spontaneous rupture of the tympanic membrane [22]. During several episodes of AOM, inflammation and continuous break-down of the collagenous layer of the TM reduces and alters the surface area of the TM which results in loss of hearing. Moreover, retraction pockets may develop as sequelae which are caused by the atrophy of the Pars

Tensa tissue [22]. The loss of collagenous fibrous layer results in thinning of the tissue which changes the structure and mechanical properties of the TM. Although the tympanic membrane has a self-healing mechanism driven by epithelial migration that can repair small perforations spontaneously [28], the repaired tissue can be flawed in terms of its layer structure.

Tympanoplasty is a clinical procedure for reconstruction of the tympanic membrane and/or ossicles, whereas Myringoplasty is an operation performed only on the TM. The damaged membrane is usually repaired with the use of graft materials taken from autologous or homologous tissues. Selection of the right graft material is critical in hearing restoration, since the selected material should have similar dynamic vibration properties. Temporalis fascia, perichondrium, and cartilage are commonly used as graft materials [29]. Among these grafts, cartilage provides higher mechanical stability with the expense of increased acoustic impedance due to higher mass and stiffness [29]. However, the disadvantage associated with autologous tissues, in general, is the risk involved with additional incision and the scarcity of the donor tissue for revision surgery [30]. Among commercial grafting materials, AlloDerm (LifeCell Corp., Branchburg, NJ) has been extensively applied in TM reconstruction. It is an acellular human derims allograft prepared from human donor skin tissues with the cellular components removed to reduce the immunogenicity [30]. However, the closure of TM perforation with the mentioned grafts cannot restore the complex microanatomy in the original TM. The apparent success in TM reconstruction can be explained by the fact that clinical audiometers generally only measure hearing frequencies up to approximately 8 KHz [2]. However, the human ear is capable of hearing up to 20 KHz. Although the frequency of human speech does not generally go beyond 4 kHz, the ability to hear higher frequencies is necessary for hearing where there is noise or multiple sources of speech [2].

2.2 Electrospinning

2.2.1 History

Electrospinning is a fabrication method for producing long and continuous nonwoven nanofibres through accelerating a charged fluid jet in an electric field gradient. The

invention of electrospinning can be traced back to the early 1900s when Colley [31] and Morton [32] used this technique to produce fibres. A few years later, Formhals devised several electrospinning set-ups to collect yarns out of electrospun fibres for textiles application. His first design was patented in 1934 [33]. A detailed list of Formhals' patents and those of other contributors to the invention of the electrospinning technique is provided by Teo *et al.* [34]. Nowadays, electrospinning is recognized as a versatile technique that has many applications including fabrication of medical materials (drug delivery materials, wound dressings, artificial organ/tissue components), composite materials, filtration devices, textiles, and energy cells [35]. A wide range of materials including polymers [35], nanoceramics and nanocomposites [36] can be used in electrospinning; however, polymer solutions are most commonly used to produce nanofibres [34]. Huang *et al.* has gathered a detailed list of all polymers that have been used, in either solution or melt form, for electrospinning [35].

There are other fabrication techniques for producing nanofibres, such as drawing, temperature-induced phase separation, and molecular self assembly [37]. However, in comparison, electrospinning is simple, inexpensive, reproducible, and versatile for the production of nanofibres as small as a few nanometers [37]. These advantages have increased the interest of many researchers in developing this process further for numerous applications.

2.2.2 Electrospinning Set-up

A typical electrospinning apparatus (Fig. 2.3) is composed of a syringe loaded with polymer solution, a syringe pump, a collector electrode and a voltage supply. The polymer solution in the syringe is continuously driven forward towards the needle tip with a constant flow rate controlled by the pump. A collector electrode, which is placed in front of the needle, is connected to a voltage supply. The needle is grounded to create an electric field gradient between the tip and the collector.
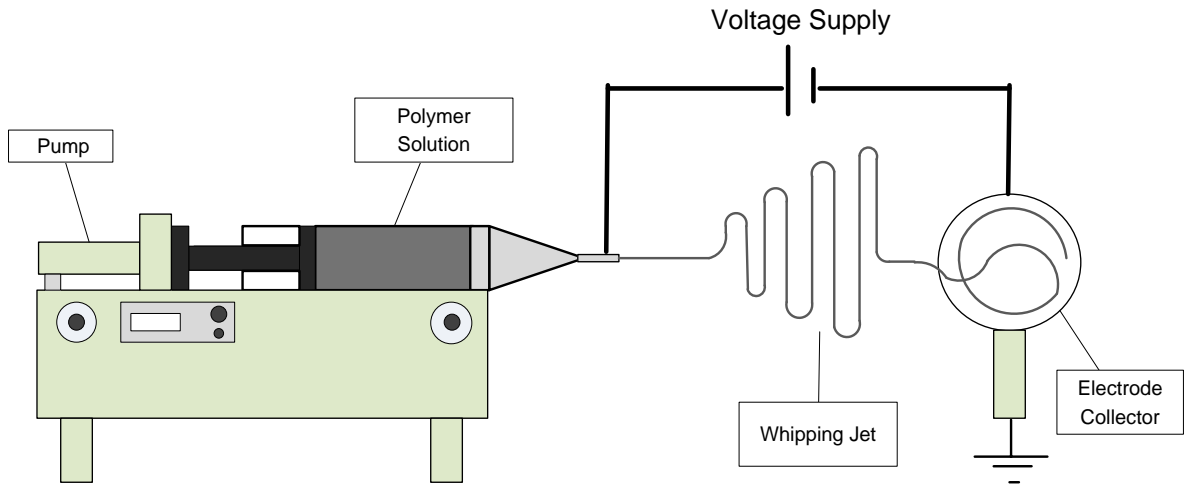
Fig. 2.3: Electrospinning set-up: syringe loaded with polymer solution, mounted on a syringe pump (left); collector electrode connected to ground (right)

The electric field introduces charge on the surface of the polymer droplet at the needle tip. As the charge density increases, the electrostatic force opposing the surface tension increases. At low voltage, the surface tension force is able to keep the polymer droplet at the needle tip. However, when the voltage exceeds a threshold value, the electrostatic force exceeds the surface tension force and the droplet at the tip forms a conical structure, called the Taylor cone [38]. Fig. 2.4 shows a schematic illustration of Taylor cone formation.
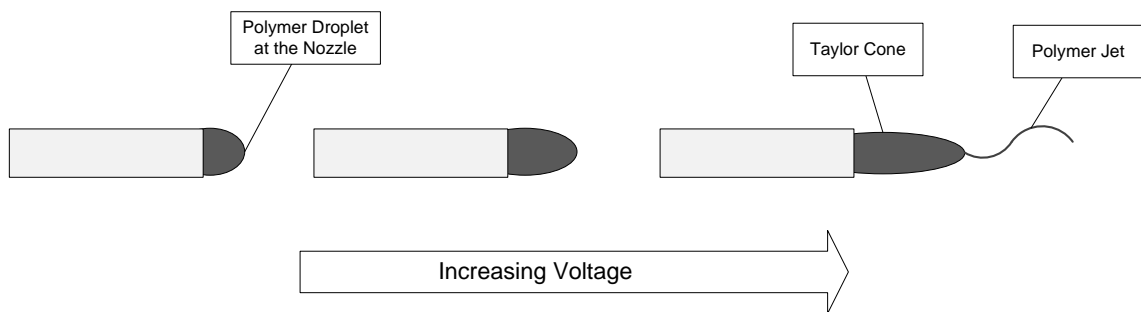
Fig. 2.4: Schematic illustration of Taylor cone formation during electrospinning

A single fluid jet is then ejected from the apex of the cone and accelerates down the electric field gradient. This leads to the rapid growth of a "whipping instability." The solvent evaporates while the jet travels through the distance between the needle tip and the collector, and the polymer strands in the jet split into nanofibres due to electrostatic repulsion.

2.2.3 Electrospinning Parameters

Electrospinning parameters should be chosen carefully since they play a significant role in the quality of the nanofibres produced. Process parameters include the applied voltage, flow rate, nozzle-collector distance, and also polymer solution properties such as polymer concentration, viscosity, conductivity, surface tension and dielectric constant. Moreover, ambient parameters (i.e., temperature and humidity) significantly affect fibre morphology. Manipulation of these parameters can result in various fibre morphologies.

Fibres with diameters ranging from 10 nm to 10 μm can be produced using the electrospinning method [39]. However, controlling the fibre diameter during electrospinning is important for many applications. Empirical observations and analytical models have been utilized to provide a quantitative prediction of the size of fibres fabricated by the electrospinning process [40, 41, 42].

Fridrikh *et al.* [43, 40] used continuum hydrodynamics to derive an equation for the diameter (*d*) of the electrospun nanofibres as a function of the surface tension (*γ*), dielectric constant (*ε*), flow rate (*Q*), the current carried by the fibre (*I*) and the ratio of the initial jet length to the fibre diameter (*X*):

$$d = (\ \gamma\varepsilon\ \frac{Q^2}{I^2}\ \frac{2}{\pi\ (2\ln X - 3)}\ )^{1/3} \qquad (1)$$

Flow rate: Empirical results have shown that lower flow rates result in smaller fibre diameter [44, 45]. On the other hand, higher flow rates create beading since the solvent does not completely evaporate and the fibres do not fully dry before reaching the collector [44, 46, 47, 48, 49].

Voltage: The strength of the electrostatic field is manipulated by the voltage supply connected to the needle. It has been found that less beading is expected when a low voltage is applied to the needle (a low but sufficient voltage so that the electrostatic force exceeds the surface tension) [44, 50]. By increasing the voltage, the Taylor cone is diminished and the jet originates from the liquid surface within the tip, causing the

formation of beads. More beading should be expected as the voltage is increased further [44, 45, 50].

Collector-Tip Distance: The influence of varying the distance between the needle tip and the collector on fibre morphology and diameter has been examined for poly(vinyl alcohol) (PVA) [46], gelatin [51], chitosan [52] and other polymers [44, 49, 53]. It was found that a minimum distance is necessary to provide sufficient time for the fibres to dry before reaching the collector [52]. Moreover, beading is observed when the collector is placed too close/far from the needle tip [44, 51, 54].

Viscosity (Concentration): One of the most influential parameters on fibre size and morphology is the polymer concentration. It has been demonstrated that for many polymers, including poly(ethylene oxide) (PEO) [55], poly(vinyl alcohol) (PVA) [46, 54], poly(methyl methacrylate) (PMMA) [56], polystyrene [57] and poly(L-lactic acid) (PLLA) [58], low polymer concentrations result in the formation of beads and defects. This process condition is known to be characteristic of electrospraying [44, 59]. On the other hand, using high concentration causes the viscous droplet dry at the tip which prevents electrospinning [44, 45, 60, 59]. Furthermore, it is found that increasing the polymer concentration yields fibres with larger diameters [51, 50, 61].

Polymer molecular weight: The effect of polymer molecular weight on the morphology and size of electrospun fibres has been investigated for many polymers [44, 56, 52, 62]. For example, for PMMA it is found that beading can be prevented by increasing the molecular weight [44, 56].

Conductivity: It has been demonstrated that increasing the solution conductivity or charge density yields more uniform fibres with less beading [44, 47, 45, 55, 63, 64]. For instance, Zhang *et al*. showed that by addition of salt to the PVA solvent, solution conductivity can be increased and fibre diameter made smaller [44, 46]. In general, smaller fibres were created by increasing the conductivity.

Dipole moment and dielectric constant: To date, only a few studies have been conducted to examine the effect of dipole moment and dielectric constant on electrospun

fibre morphology since it is very difficult to investigate these parameters independently [44, 57].

Surface tension: The impact of surface tension on fibre morphology and diameter size has been studied for PVA and PEO. However, no conclusive link is established [44, 46, 64, 47].

Ambient Parameters: To date, only a few studies have been conducted to investigate the effect of ambient parameters on morphology and size of electrospun fibres. Mit-Uppatham *et al.* reported that increasing the temperature yielded fibres with smaller diameter for polyamide-6 [44, 63]. Also, Casper *et al.*'s study on polystyrene solution revealed that increasing the humidity results in formation of pores on the surface of fibres [44, 65].

2.2.4 Fibre Alignment

A simple stationary collector electrode placed in front of the needle collects fibres with random alignment. However, for many applications, it is required to control the alignment of fibres in the electrospun fibrous mats. For example, patterned architectures of the fibrous mats can enhance cell attachment and proliferation and can greatly impact the biological responses in newly regenerated tissues [66, 67, 68]. Several research groups have examined different collector designs to control the 2D or 3D orientation of electrospun fibres. Li. *et al.* demonstrated that a collector with two parallel pieces of conductive silicon strips separated by a void gap (Fig. 2.5-A) can be used to collect uniaxially aligned fibres [69].
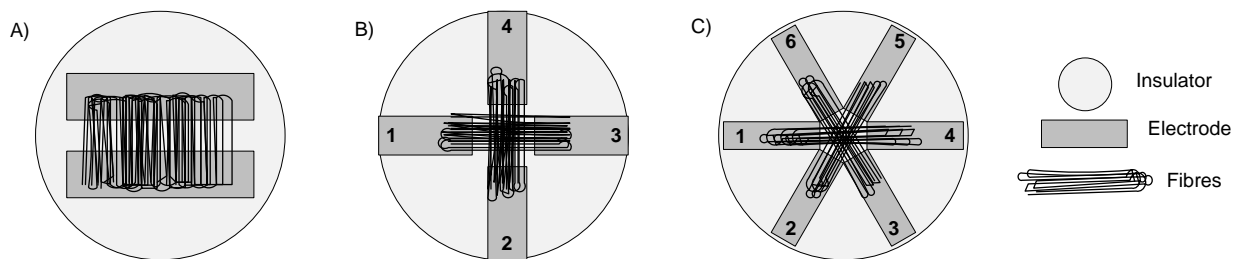
Fig. 2.5: 2D Architecture of electrospun fibres on: A) two parallel electrodes, B) four electrodes, C) six electrodes (adapted from [69, 70]).

Li. *et al.* explained the mechanism of this alignment by looking at the electrostatic interactions between the fibres and the surrounding electric fields. The motion of an ejected electrospun fibre is controlled by the electrostatic forces exerted from the strong field created by the voltage supply and the collector, and the adjacent charged fibres [69]. When a continuous collector electrode (i.e., with no gap) is used, the electrostatic forces have no preferential direction and cause random deposition of fibres. However, when two conductive strips with an insulating gap are used, the electric field is altered, causing a different motion and alignment of fibres [69]. Also, the electrostatic repulsive interactions between the deposited fibres impact the alignment. Unlike continuous electrodes which result in immediate discharge of fibres, electrodes with an insulator gap result in parallel deposition of fibres which remain highly charged after contacting the electrodes. The electrostatic repulsion of fibres with the same charge results in deposition of fibres with parallel alignment to reach the lowest possible state of energy [69]. Li. *et al.* also used this approach to deposit electrospun fibres with different patterns on multiple electrodes, as shown in Fig. 2.5-B, C. One electrode for each pair (1 or 4, 2 or 5, 3 or 6 in Fig. 2.5-C) was grounded for 5 s to collect fibres spanning over the two electrodes and the collector was rotated approximately by 60 degrees sequentially to collect fibres on all electrodes [69].

In addition, controlling the 3D structure of electrospun fibrous mats has also been investigated by several research groups for biomedical applications such as tubular scaffolds. Zhang *et al.* demonstrated a novel approach to control the alignment of fibres in 3D electrospun cylindrical mats [67]. They used the principles of Coulomb interactions; similar to the principles that Li *et al.* used for fabrication of aligned 2D structures. Zhang *et al.* used tubular structures with patterns protruding from the surface to fabricate patterned nanofibrous cylindrical scaffolds [67]. In another study, Xu *et al.* used a rotating disk (Fig. 2.6.b) with sharp edge to fabricate three-dimensional nanofibrous scaffolds using electrospinning [71]. Pan *et al.* and Wang *et al.* used different approaches to collect electrospun fibres as yarns by inducing self-bundling, and used a rotating drum (Fig. 2.6.a) to collect the yarns [72, 73]. In all these studies, it was found that the speed of the rotating collector was an influential parameter in determining the degree of alignment.
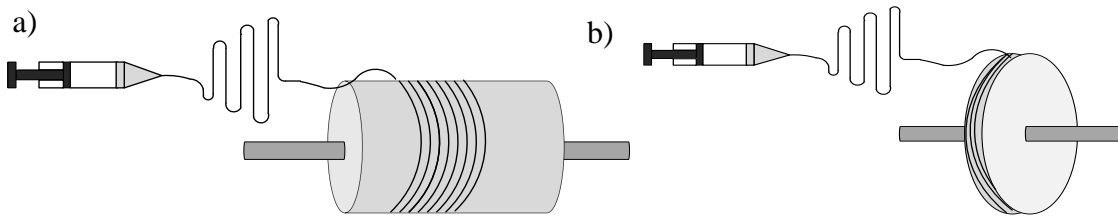
Fig. 2.6: Rotating drum (a) and disk (b) for collecting 3D nanofibrous structures using electrospinning (adapted from [71, 73])

2.2.5 Coaxial Electrospinning

Coaxial electrospinning produces hollow or core-shell nanofibres that can be used for encapsulation of biological molecules. For controlled release applications, proteins [74, 75] and drugs [76] have been successfully encapsulated in polymeric core-shell fibres using coaxial electrospinning.

The apparatus is similar to the conventional electrospinning set-up, as illustrated in Fig. 2.7. Two syringes loaded with core and shell solutions are mounted on a dual pump. The solutions are fed into a spinneret using a capillary tube. An electric field is induced between the spinneret and the electrode collector, which results in formation of core-shell fibres.
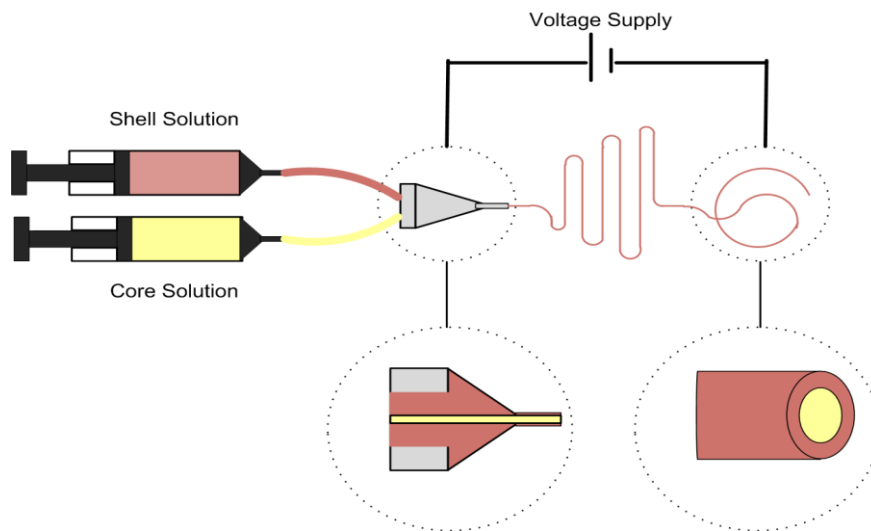
Fig. 2.7: Coaxial electrospinning set-up: Syringes loaded with core and shell solution feeding into one spinneret via capillary tubing

2.3 Materials for Electrospinning

2.3.1 Poly(caprolactone)

Poly(caprolactone) (PCL) is a biocompatible and biodegradable aliphatic polyester which is hydrophobic. It has several FDA-approved biomedical applications such as medical sutures and drug delivery devices [10]. PCL is considered as an attractive biomaterial, since after degradation by hydrolysis of its ester linkages, its by-products are neutral and do not change the pH of the natural environment [11]. Fig. 2.8 shows the chemical structure of PCL which is synthesized by the ring-opening polymerization of ε-caprolactone.
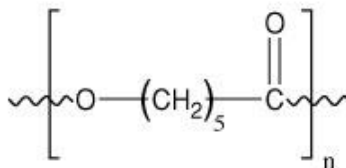
Fig. 2.8: Chemical structure of Poly(caprolactone)

2.3.2 Trifluoroethanol

Trifluoroethanol (TFE) is a water soluble organic solvent which can dissolve peptides and proteins. Its chemical structure consists of an electronegative trifluoromethyl group which is beneficial for the electrospinning process, since it is repelled by the positive charge at the needle tip. TFE is less volatile than other organic solvents and has been successfully used in electrospinning to dissolve PCL [77, 78]. The chemical structure of TFE is shown in Fig. 2.9.
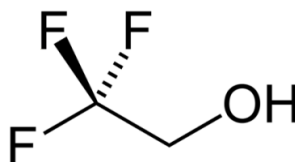
Fig. 2.9: Chemical structure of TFE

2.3.3 Poly(ethylene glycol)

Poly(ethylene glycol) (PEG) is a polyether with low toxicity which is utilized in a variety of medical applications. Also, since it is flexible and water-soluble, many researchers have used it in coaxial electrospinning [74, 77]. By incorporating it in the core solution, pores are created in the shell of the core-shell or hollow fibres. Porous fibres are used in controlled drug delivery systems (DDS) [79, 77, 80].
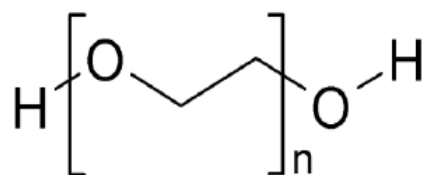
Fig. 2.10: Chemical structure of poly(ethylene glycol)

2.3.4 Collagen

Collagen is the most abundant protein in mammals, and is present in several tissues, such as tendons, ligaments, cartilage, bone, cornea, dentin, skin, arteries, and the extracellular matrix. The molecule of collagen comprises three polypeptide chains, called α chains; each of which has the repeating (Gly-X-Y) amino acid motif, where the residues X and Y can be any amino acid [81]. The chains form a right-handed, triple helical structure with the X and Y groups protruding from the surface, and all the glycine residues facing the core. High content of proline and hydroxylproline residues (approximately 20% of the total amino acids in human fibrillar collagens) is reported to be important for the stability of collagen triple helix [81]. As illustrated in Fig. 2.11, the three polypeptide chains combine to create the tropocollagen molecule, which is a right-handed coil with tertiary structure. A group of staggered tropocollagen molecules then combine to create collagen fibrils.
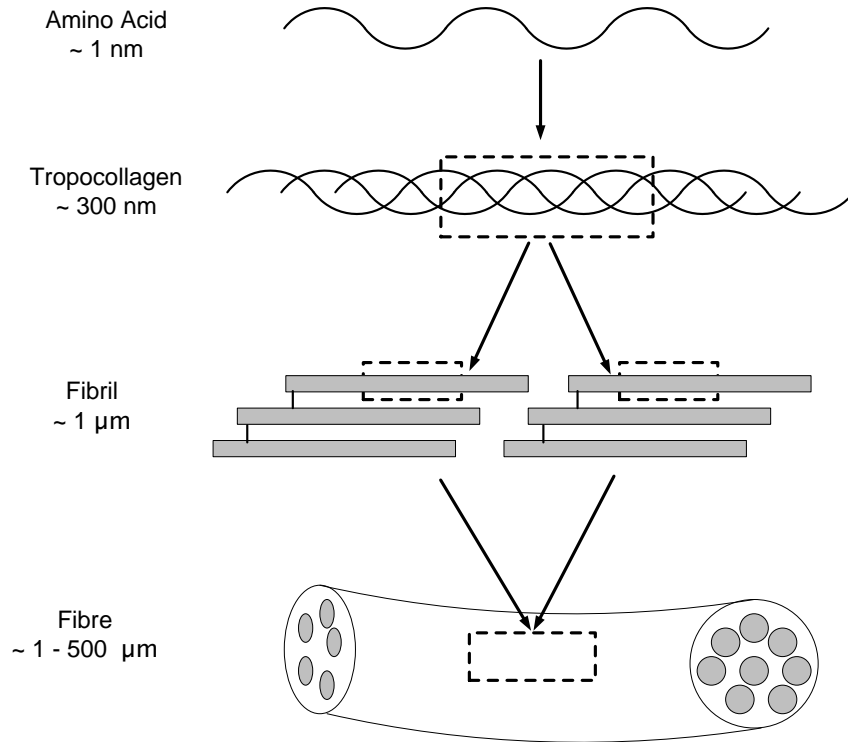
Fig. 2.11: Collagen's hierarchical structure (adapted from [82, 83])

There are 28 different types of proteins in humans which are known as collagen [81]. Collagen is classified into different subfamilies such as fibrillar collagens, basement membrane and associated collagens, transmembrane collagens, and short chain collagens [81]. Different types of collagen in each subfamily are numbered with roman numerals. For instance, fibrillar collagen type I is present in many tissues including skin, tendon, bone, and cornea.

Mechanical properties of numerous tissues are attributed to the presence of collagen fibres. These fibres play a significant role in load-bearing tissues such as ligaments and tendons, in the organic matrix of the stiff bone and dentin, and in the soft cartilage. Various mechanical properties (i.e., strength, stiffness, toughness) are attributed to the presence of collagen because of the versatility of collagen as a building material. Hierarchical assembly of collagen fibres in different tissues lead to their unique mechanical properties. Moreover, the presence of minerals as inclusions in tissues can lead to high stiffness, as seen in bone and dentin [81].

Collagen is considered a promising biomaterial for creating tissue engineering scaffolds because of its biocompatibility and its unique mechanical properties. To date, several studies have reported promising results of electrospun collagen fibres for tissue engineering applications [14]. However, upon exposure to aqueous environment, as-spun collagen fibres disintegrate and lose their mechanical stability. As a result, post fabrication cross-linking is necessary for stabilization [14]. Two conventional materials that have been applied to stabilize collagen are glutaraldehyde (GA) and 1-ethyl-3-(3-dimethylaminopropyl) carbodiimide (EDC) and N-hydroxysuccinimide (NHS).

Glutaraldehyde is considered as an important cross-linking agent for the preparation of biomedical devices such as heart valves, vascular grafts, and artificial skin [84]. Compared with other cross-linking aldehydes, GA can react relatively quickly in a protein matrix, and is able to react with larger number of amino groups [85, 86]. As a result, the cross-linked network will be tighter. However, residual GA in bioprostheses and unstable GA polymers remaining in the interstices of cross-linked matrices have been reported as the main cause of biological responses of cytotoxicity and calcification [87]. On the other hand, the major problems reported for EDC-NHS are significant swelling and loss of fibre morphology and porosity [88]. Mekhail *et al.* investigated the effect of genipin, a less cytotix cross-linking agent, on maintaining collagen fibres integrity in cell culture media [89]. Cell compatibility was also assessed using primary human fibroblasts cultured in genipin-cross-linked collagen scaffolds which showed successful cell adhesion to the stabilized collagen nanofibres [89].

2.4 Mechanical Testing Technique

The overall mechanical properties of a fibrous scaffold is a function of the mechanical properties of individual fibres and the alignment of fibres within the scaffold [90]. The Young's modulus of electrospun fibrous mats has been measured by several research groups using the conventional uniaxial tensile testing technique [91, 92]. Moreover, several other groups have measured the Young's modulus of single fibres greater than 1 µm using the conventional tensile method [93, 94]. However, this technique is not applicable for measuring fibres in the nanometer range, due to inadequate sensitivity of the instrument. Other limitations include the difficulty of proper gripping the two ends of

small fibres with no damage or slipping from the grip, and the perfect alignment of the fibre with the loading direction to avoid unwanted bending moments [95]. To overcome these obstacles, numerous mechanical characterization techniques have been proposed by different researchers which are based on tensile, stretching, resonance excitation and bending of fibres as depicted in Fig. 2.12.
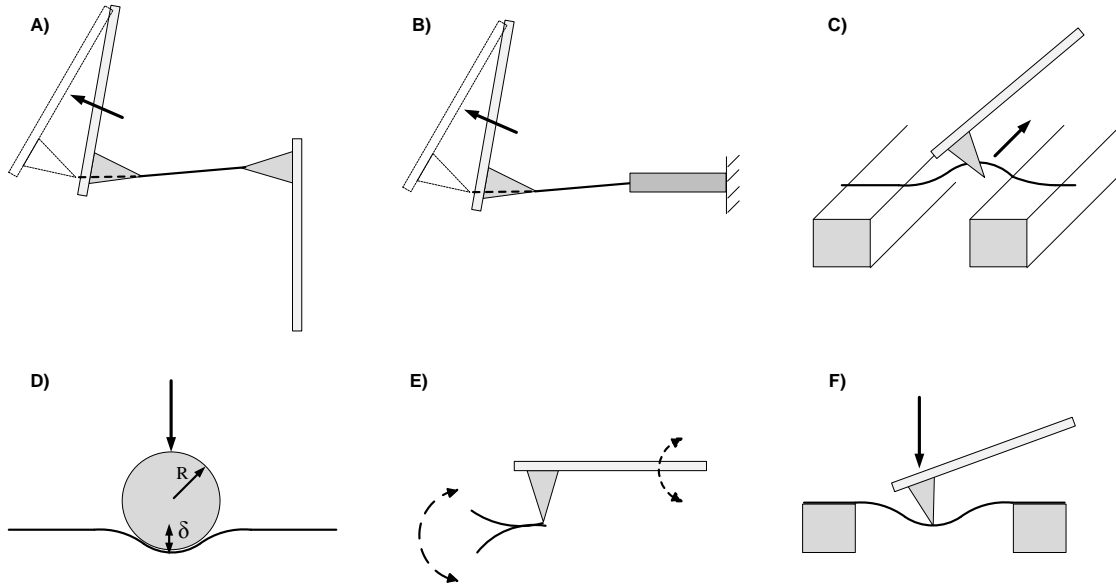
Fig. 2.12: Schematic illustration of different techniques for mechanical characterization of nanofibres: A) and B) tensile testing, C) stretching, D) nanoindentation, E) resonance excitation, F) bending (adapted from [14, 62-65])

2.4.1 Tensile Tests

To overcome the challenges associated with conventional tensile testing, several research groups have utilized AFM cantilevers to perform the tensile test. Ding *et al.* used this technique to investigate the elastic modulus of boron nanowires [96]. They clamped each end of a single nanowire to the tip of a soft and a rigid cantilever which were positioned parallel to one another but with opposite orientation, as shown in Fig. 2.12-A. A piezoelectric bender was then used to gradually pull the soft cantilever away from the rigid one to stretch the nanowire until fracture. The stress-strain behaviour was determined from the length of the nanowire which was frequently measured using a series of images that were taken during tensile loading, and the applied tensile force

which was determined from the cantilever's deflection and its spring constant [96]. In a similar study, Zussman *et al.* mounted one end of an electrospun Nylon-6,6 nanofibre to a stainless steel wire and pulled the other end which was attached to a cantilever tip [15], as illustrated in Fig. 2.12-B. The deflection of the cantilever and the elongation of the nanofibre were monitored using a microscope, and the stress-strain curve was obtained to determine the Young's modulus and mechanical strength of the nanofibres [15]. The disadvantage of these cantilever-based tensile testing techniques is that they are time consuming and difficult to manipulate single fibres.

2.4.2 Stretching

Baker *et al.* used a combined AFM/optical microscope to examine the elasticity of single electrospun fibrinogen fibres [97]. The AFM tip was used to pull the fibre laterally with a constant rate and an optical microscope was used to monitor the resulting stretching of the fibre. The elapsed time and the distance traveled by the tip were also recorded and used to calculate the fibre's elastic properties [97]. The schematic illustration of this technique is shown in Fig. 2.12-C. Hwang *et al.* also used a similar technique by utilizing a nanomanipulator and an AFM cantilever in scanning electron microscope (SEM) to stretch a Nylon 6 electrospun nanofibre suspended over a trench in the transverse direction [98]. However, there are a few challenges associated with this technique. The experiment should be conducted as fast as possible inside SEM to prevent heating and charge build-up in samples [98]. Also, fixing the two ends of a nanofibre using clamps or adhesive materials is a time consuming process.

2.4.3 Nanoindentation

Nanoindentation is a nanomechanical characterization technique which has been used in several studies to examine the elastic and elastic-plastic behaviour of nanowires and nanofibres [95, 99]. The sample can be simply prepared by depositing a nanowire on a flat and rigid substrate with sufficient adhesion to the substrate. The Young's modulus can then be obtained through probing the localized curvature created on the surface of the fibre after indentation (Fig. 2.12-D). Li *et al.* used an AFM-based nanoindentation system to investigate the elastic-plastic behaviour of silver nanowires [95, 99]. Immediately after

indentation, an image of the indented area was captured to determine the elastic modulus. In a recent study, Clifford *et al.* used the AFM nanoindentation technique to investigate the modulus of hair as a micro-fibre. They demonstrated that the ratio of the radii of the tip and the fibre significantly impacts the nanoindentation measurements [100]. Tan *et al.* has summarized other important factors which are critical in nanoindentation experiments [95]. These factors include the substrate under the fibre, the cantilever's spring constant and the tip radius, the fibre's surface roughness, slipping and friction between the tip and the fibre's surface caused by loading in non-perpendicular direction, and the effect of capillary forces due to humidity [95].

Nanoindentation is one of the easiest nanomechanical characterization experiments that can be performed on a nanofibre; however, it provides limited information about the mechanical properties of samples compared with other techniques [95]. Furthermore, only fibres larger than 200 nm can be characterized using this method [95]. When the sample thickness is very small, the nanoindenter's tip can "feel" the underlying substrate after compressing the sample. As a result, an overestimated value of the Young's modulus will be obtained [101, 95].

2.4.4 Resonance Excitation

The mechanical resonance technique is a non-destructive method that applies an electrically or mechanically induced periodic force (approaching the nanowire's resonance frequency) for excitation of a nanowire clamped to the tip of a cantilever (Fig. 2.12-E) inside a scanning electron microscope (SEM). The resulting frequency responses of the nanowire are then recorded and the resonance peaks are obtained to calculate the Young's modulus. Ding *et al.* [96] and other research groups have used this technique to investigate the mechanical properties of nanowires [102, 96], nanotubes [103, 104, 96], and nanobelts [105, 96]. However, there are a few challenges associated with this technique. First, it is difficult to manipulate single fibres and clamp them to a cantilever's tip. Also, it is reported that electrical excitation introduces an additional electric field in the SEM which results in lower image quality [96]. As a result, electrical excitation cannot be used for very stiff samples (i.e., with small vibration amplitude), since they require strong electric fields [96].

2.4.5 Bending Tests

Most bending techniques reported in the literature are three-point bending tests (Fig. 2.12-F) that have been performed on suspended nanofibres spanning a gap, with their two ends fixed on a substrate, in accordance with Euler-Bernoulli beam theory [20], as applied to the clamped-beam model. The elastic modulus of these fibres was determined by measuring the deflection of the fibres after an AFM tip applied a force at the centre point of the suspended fibres [19, 106, 107]. Guhados *et al.* introduced a multi-point bending test based on the concept of three-point bending [21]. In Guhados *et al.*'s bending method, a known force was applied by the cantilever at multiple points along a suspended fibre while the deflection of the fibre was measured and recorded for each point. The multi-point bending test eliminates the need for finding the exact centre point of the fibre. It is also easier to verify whether the boundary conditions meet those of the clamped-beam model [21].

Several models can be applied to analyze the behaviour of a beam under loading. However, these models differ in their assumptions and the level of accuracy. The Euler-Bernoulli model [20] is one of the simplest models, and was developed based on the assumption that the beam's deflection is small enough that the restoring force is only due to the compressive and tensile stresses along the axis of the beam. These assumptions are valid for long, slender beams of isotropic materials with uniform solid cross section [20]. In Euler-Bernoulli model, which is often known as the "pure bending" model, there are only two bending moments applied at the ends and the properties of the beam are considered constant along its span. Fig. 2.13 depicts a section of a deformed beam under compression above the neutral axis *N*, and under tension below *N*.
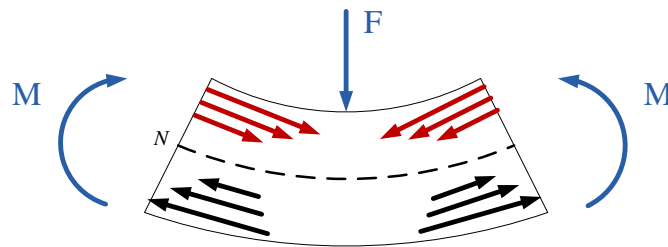
Fig. 2.13: Schematic illustration of compression (above neutral axis *N*) and tension (below neutral axis *N*) as a result of two bending moments

Timoshenko's beam theory is an extension of Euler-Bernoulli model which considers the effect of shear in the beam's deformation. The assumption is that during bending of the beam, the cross section remains planar but not perpendicular to the neutral axis [108]. The Euler-Bernoulli and Timoshenko's beam models are both based on the assumption that the length of the beam does not change during bending experiments. However, in reality, deflection increases the length, which in turn induces axial tensile stresses in the beam. As a result, the total stress experienced by the beam will be different and the rigidity of the beam will be increased [109]. Heidelberg *et al.* has provided a model to determine the elastic properties of nanowires by considering the effect of tension [109].

2.5 Tissue Engineering

2.5.1 Introduction

Regenerative medicine combines the principles of human biology, materials science, and engineering to restore, maintain or improve a damaged tissue function. Regenerative medicine is divided into cell therapy, or "cell transplantation," and "tissue engineering" [110]. Cell transplantation is performed when only cell replacement is required. However, in tissue engineering, the generated tissue should have similar properties to the native tissue in terms of biochemical activity, mechanical integrity and function. This necessitates providing a similar biological environment as that in the body for the cells to generate the desired tissue. Fig. 2.14 summarizes the important steps in tissue engineering. First, cells are harvested from the patient and are expanded in cell culture medium. After sufficient expansion, the cells are seeded into a porous scaffold along with signaling molecules and growth factors which can promote cell growth and proliferation. The cell-seeded scaffold will be then placed into a bioreactor before being implanted into the patient's body. As it is evident in Fig. 2.14, three major elements of tissue engineering include:

- Cells
- Scaffolds
- Bioreactors
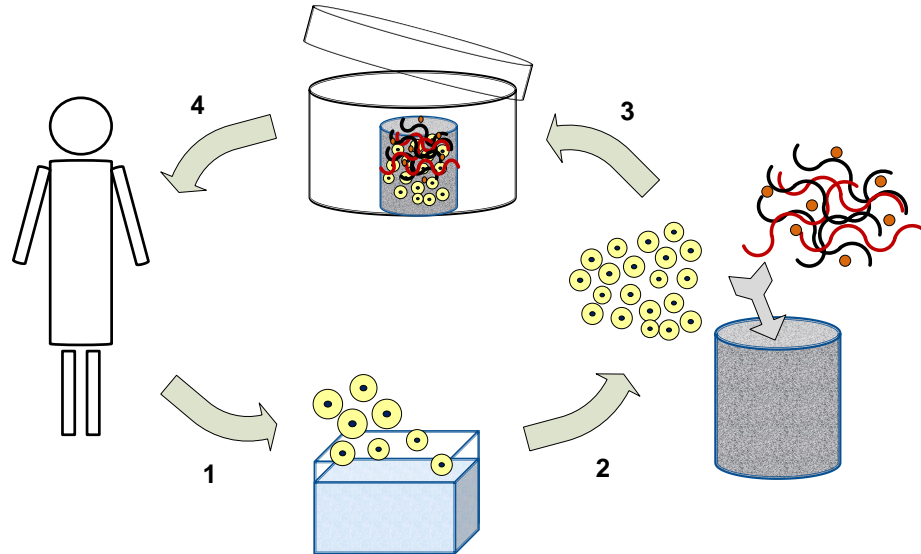
Fig. 2.14: Schematic diagram summarizing the tissue engineering process

2.5.2 Cells

Cells are the building block of all tissues. Therefore, choosing the right cell source with no contamination that is compatible with the recipient's immune system is the critical step in tissue engineering. Stem cells are employed as the main source of cells for tissue engineering and are taken from autologous, allogeneic or xenogenic sources for different applications. Stem cells are divided into the following three groups: embryonic stem cells (ESCs), induced pluripotent stem cells, and adult stem cells [111]. ESCs are isolated from the inner cell mass of pre-implantation embryos. These cells are considered pluripotent since they can differentiate into almost any of the specialized cell types [111]. Induced pluripotent stem cells are the adult cells that have been transformed into pluripotent stem cells through programming. Among adult stem cells, Mesenchymal stem cell is widely used as a multipotent source [111]. Mesenchymal stem cell is derived from bone marrow stroma and can differentiate into a variety of cell types *in vtiro*. Other sources of adult stem cells include the amniotic fluid and placental derived stem cells [111].

2.5.3 Scaffolds

The extracellular matrix (ECM) provides the necessary signals to orchestrate cell activities such as migration, adhesion, differentiation, and proliferation. The three-dimensional structure of the ECM provides structural clues for the cells to carry out their activities. When the ECM is damaged or lost, not only the cells but also the matrix in tissue is lost. As a result, to support the cells and to promote tissue regeneration, the replaced artificial material should mimic the 3-D spatial organization of ECM [110].

Cell culture studies require a solid substrate for cell adhesion in order to promote cell proliferation, since cells do not survive when suspended in fluid medium [8]. Scaffolds are temporary porous structures used to support cells by filling up the space otherwise occupied by the natural ECM and by providing a framework to organize the dissociated cells. A biocompatible and biodegradable material is chosen for tissue engineering scaffolds which have sufficient porosity and pore-interconnectivity to promote cell migration and proliferation, and allow for nutrient and waste exchange. The rate of degradation should be tuned with the rate of cell growth and expansion, so that as the host cells expand and produce their own ECM, the temporary material degenerates with a similar rate. Moreover, the by-products should be confirmed to be non-toxic. Mechanical properties should also match that of the native ECM. However, as it is illustrated in Fig. 2.15, it is necessary that these properties deteriorate as the cells build their own ECM. Furthermore, sufficient stimuli should be provided to encourage and direct cell growth, particularly in load-bearing tissues.
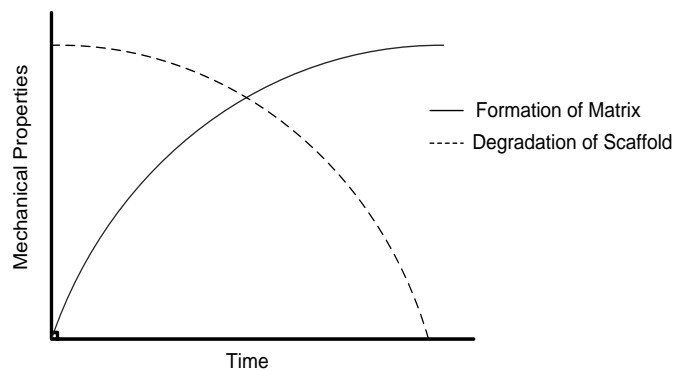
Fig. 2.15: Mechanical properties of an ideal scaffold (adapted from [112])

2.5.4 Bioreactors

In-vitro tissue engineering requires bioreactors in order to provide sufficient nutrients and oxygen to the cells while removing the toxic materials left by the proliferating cells. Moreover, the essential cell-specific mechanical stimuli are also provided by bioreactors. Each type of cell (cartilage, bone, myocardium, endothelial, etc) has different requirements in terms of pH, oxygen tension, mechanical stimulation, temperature, etc. As a result, it is necessary to use cell specific bioreactors for generation of different tissues [113, 114].

Chapter 3: Materials and Methods

3.1 Materials

The following materials (Table. 3.1) were purchased for electrospinning and characterization of solid and core-shell PCL and collagen (as-spun and cross-linked) nanofibres:

Table. 3.1: Materials for electrospinning and characterization of PCL and collagen fibres

Material	Supplier	Specification	Item Number
Poly (ε-Caprolactone) (PCL)	Sigma Aldrich*	80 kDa	440744
Trifluoroethanol (TFE)	Sigma Aldrich	2,2,2-TFE Reagent Plus®	T63002
Poly (Ethylene Glycol) (PEG)	Sigma Aldrich	10 kDa	309028
Fluorescein Isothiocyanate labelled Bovine Serum Albumin (FITC-BSA)	Sigma Aldrich	λmax = 495 nm	A9771
Prolong Gold Antifade Reagent	Invitrogen	1.47 RI	P36930
Type I Collagen	Sigma Aldrich	Type I from Rat Tail	C7661
Hexafluoroisopropanol (HFIP)	Sigma Aldrich	1,1,1,3,3,3-hexafluoroisopropanol	105228
Ethanol	Caledon Laboratories**	> 95%	1500-1
Albumin From Bovine Serum	Invitrogen Canada Inc***	Alexa Fluor® 594 conjugate	A13101
Genipin	Challenge Bioproduct Co.	MW = 226.23g/mol	_____

*Sigma Aldrich (Oakville, ON, Canada), **Caledon Laboratories (Georgetown, ON, Canada), ***Invitrogen Canada Inc (Burlington, ON, Canada)

3.2 Solutions

3.2.1 PCL Solution

Homogeneous PCL solution (12 wt%) was prepared by dissolving 1.2 g of PCL in 10 mL of TFE for 6 hours at room temperature.

3.2.2 Collagen

Type I collagen solution (5 wt%) was prepared by adding 84.2 mg of type I collagen from rat tail to 1 mL of HFIP, and vortexing at room temperature for approximately 2 hours.

3.2.3 Protein Core Solutions

Bovine Serum Albumin (BSA) solutions with concentrations of 10 mg/mL were prepared as previously established [115, 116] . The solution was prepared by dissolving 100 mg of BSA in 10 mL of double distilled water to obtain a concentration of 10 mg/mL. In order to provide stability and to prevent mixing during the electrospinning process, poly (ethylene glycol) (PEG), with molecular weight of 10 kDa, was dissolved into the BSA core solution to achieve a final concentration of 200 mg/mL.

Previous work demonstrated that fluorescently tagged albumin proteins could be added to the core solution in order to verify the formation of core-shell structure using confocal microscopy [115]. For PCL fibres, the core solution was prepared by dissolving BSA-FITC (ex. 495 nm, em. 520 nm) in 1 mL of double distilled water to achieve a concentration of approximately 10 µg/mL. PEG was then added to the solution to obtain a final concentration of 200 mg/mL. For collagen fibres, the core solution was prepared by dissolving PEG into 95% ethanol to obtain the final concentration of 200 mg/mL. Small amount of BSA-Alexa Fluor 594 (ex. 590 nm, em. 617 nm) was then added to the solution to obtain an approximate concentration of 10 µg/mL. The solutions were wrapped in aluminum foil and stored at 4°C.

3.2.4 Genipin Cross-linking

Genipin with concentration of 0.03 M was prepared to stabilize electrospun collagen fibres as previously established [89]. Cross-linking solution was prepared from 100% ethanol, 5% water in solution, and 11.3 mg of genipin per 1 mg of collagen. The electrospun collagen fibres were placed in vials containing 10 mL of the cross-linking solution. The vials were covered with aluminum foil and placed in water bath at 37 °C for five days to speed up the cross-linking reaction.

3.2 Electrospinning Set-up

3.2.1 Electrospinning Solid Fibres

A syringe pump (Model 33, Harvard Apparatus) was used for electrospinning solid PCL and collagen fibres. A voltage source (Glassman High Voltage Inc.) was connected to the needle (30 gauge) of the syringe to create a voltage of $10 - 20$ kV. A custom designed stationary collector electrode was placed $10 - 15$ cm in front of the needle tip and connected to ground. For electrospinning collagen fibres, the collector electrode was placed inside a custom-made humidity controlled chamber (RH: 20–25 %). The needle was inserted into the chamber through an outlet which was perfectly sealed in order to isolate the electrospun fibres from the ambient environment. Fig. 3.1 shows the custom designed electrospinning apparatus.
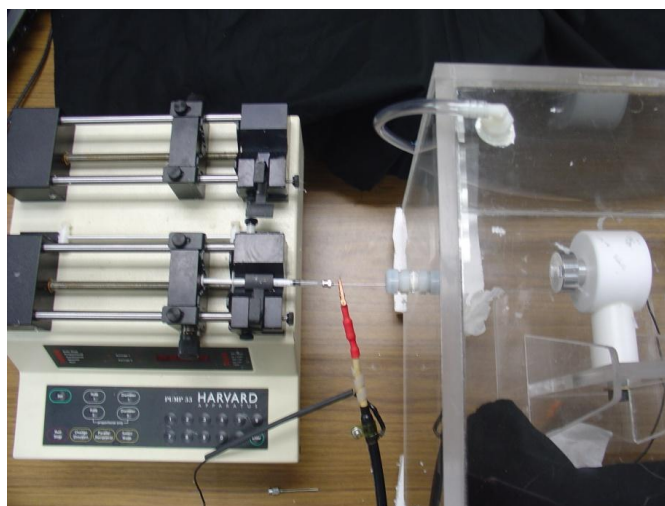
Fig. 3.1: Custom designed electrospinning set-up

3.2.2 Coaxial Electrospinning

The coaxial electrospinning set-up was assembled as previously established [116]. The dual syringe pump (Model 33, Harvard Apparatus), shown in Fig. 3.1, was used to control the flow rate of the core and shell solutions independently. The two solutions were fed concentrically into a single spinneret using flexible silica capillary tube with inner diameter of 250 µm. The capillary tube was inserted into a plastic syringe and threaded into a 20-gauge metal needle. The voltage source and electrode collector were the same as those used in electrospinning solid fibres.

3.3 Electrospinning Parameters

Experimental parameters (i.e., voltage, flow rate, needle-collector distance) and the combination of variables for electrospinning solid and core-shell PCL and collagen nanofibres are summarized in Table. 3.2, as previously established [115].

Table. 3.2: Electrospinning parameters of solid and core-shell PCL and collagen nanofibres

Fibre Type	Voltage (kV)	Flow Rate(mL/hr)	Needle-Collector Distance (cm)
Solid PCL	12-20	0.1	10-15
Core-Shell PCL	15	OFR*: 0.3, IFR**: 0.1	10-15
Solid Collagen	18	0.25	10-15
Core-Shell Collagen	11-13	OFR: 0.18, IFR: 0.06	10-15

*OFR: Outer Flow Rate (Flow rate of shell solution), **IFR: Inner Flow Rate (Flow rate of core solution)

3.4 Imaging Techniques

3.4.1 Scanning Electron Microscopy (SEM)

A SEM Hitachi 3400s scanning electron microscope was used to obtain images of solid PCL and collagen fibres. The fibres were not sputter coated and were kept intact during imaging by using low accelerating voltage of 2-3 kV. The obtained SEM images were

utilized to characterize the fibre morphology, and were used as a map to track single suspended fibres crossing the trenches.

3.4.2 Transmission Electron Microscopy (TEM)

A Philips CM10 transmission electron microscope was used to obtain images of core-shell PCL and collagen fibres. The electrospun fibres were collected directly on a TEM grid. Use of 80 – 100 kV provided sufficient energy to capture high resolution images with no excess charging and damage to the fibres. TEM images were used to characterize the core-shell fibre morphology and to measure the inner and outer diameter of hollow fibres.

3.4.3 Laser Scanning Confocal Microscopy (LSCM)

A Carl Zeiss Laser Scanning Confocal Microscope (LSM 510 Duo Vario) equipped with an Argon/He/Ne laser was used to image core-shell PCL and collagen fibres loaded with a fluorescently tagged protein. The excitation and emission wavelengths of BSA-FITC (used in PCL fibres) are 495 nm and 520 nm and Alexa Fluor 594 (used in collagen fibres) are 590 nm and 617 nm, respectively. LSCM images were obtained to verify the existence of encapsulated fluorescently labeled proteins inside fibres and the formation of core-shell structure.

3.5 Atomic Force Microscopy

3.5.1 Fundamentals

A simple schematic illustration of the atomic force microscope (AFM) is shown in Fig. 3.2. The cantilever has a sharp tip (less than 100 Å in diameter) which is located at its free end and is typically 100–200 μm in length. Topographical images of samples are obtained by sliding the probe's tip across the surface. The interaction of several forces between the tip and the sample surface contribute to the deflection of the cantilever. As the cantilever deflects while probing the surface, a photo detector monitors the position of a laser beam reflecting from the cantilever. A map of surface topography is obtained using the information acquired from the detector.

The forces which act between the tip and the sample surface include the interatomic force, known as the van der Waals force. Capillary forces may also appear due to the presence of a thin layer of water wicking around the tip when AFM imaging is performed.
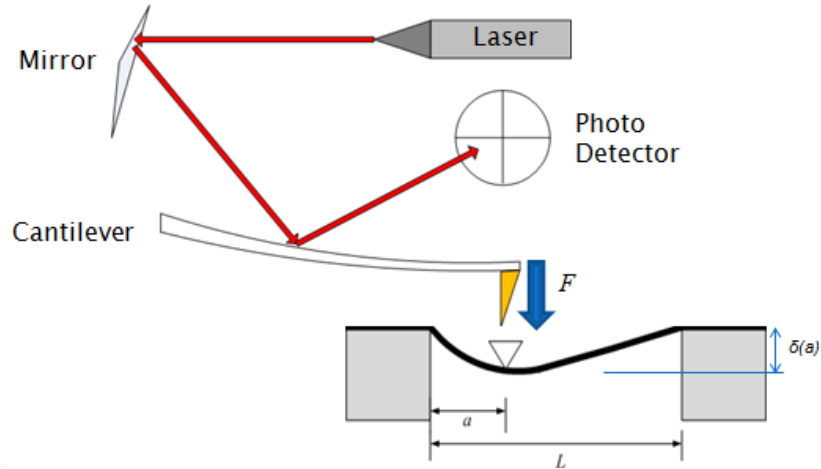
Fig. 3.2: Major components of an atomic force microscope (AFM)

Nanoscope controller 8.15 was used to obtain high resolution topographical height images of samples using contact mode in air. The force volume mode was used to acquire force curves to investigate the elastic modulus of single fibres at ambient conditions. A silicon nitride cantilever with a nominal spring constant of 0.12 N/m was used to test the elasticity of fibres.

3.5.2 Sample Preparation

All fibres were deposited on custom-designed silicon substrates with several trenches (depth = 2μm). Trenches were fabricated by photolithography and reactive ion etching at the Western Nanofabrication Facility (London, Canada), using a custom-designed mask produced at the University of Alberta NanoFab facility (Edmonton, Canada).

Prior to mounting the samples in the atomic force microscope, SEM images of samples were captured using SEM Hitachi 3400s. The fibres were not sputter coated and were kept intact using a low accelerating voltage (3 kV). Fig. 3.3 is an example SEM image of PCL fibres on the silicon substrate. To reduce the time needed to find single suspended fibres crossing a trench during the AFM mechanical testing, trench numbers and the

precise location of single suspended fibres on each trench were used to locate fibres for subsequent AFM contact imaging.
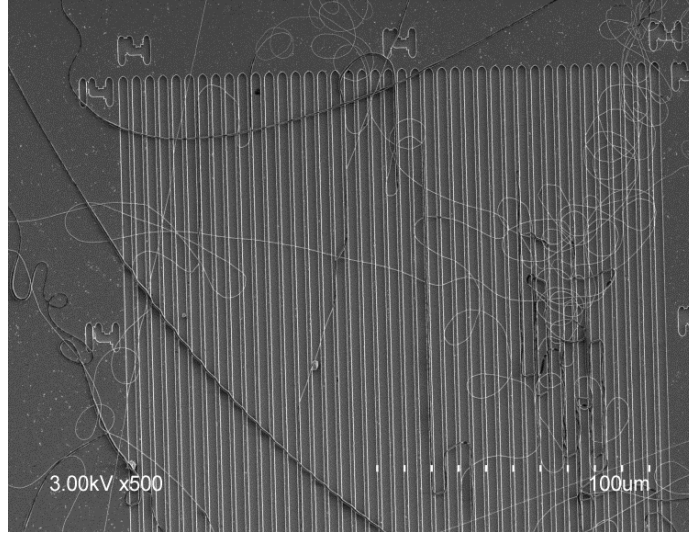
Fig. 3.3: SEM image of electrospun PCL fibres collected
on custom-designed silicon substrate

3.5.3 Cantilever Selection & Calibration

Equation 3.3 was used to select cantilevers with spring constants approximating the predicted value of F/δ (N/m) for the fibres being probed. Triangular Si_3N_4 cantilevers (Sharpened NP Probes, Veeco Instruments) with nominal spring constant of 0.12 N/m were chosen for AFM imaging and mechanical testing. The actual spring constant was frequently measured with the thermal noise calibration technique using Nanoscope controller 8.15.

3.5.4 Force Volume Measurement

AFM force volume mode was used to perform the mechanical testing as previously established [21]. A force (F) was applied to the sample at multiple points along each suspended fibre as the piezo moved the sample upward toward the AFM tip. The deflection of the cantilever (Δy) as a result of the vertical displacement of the sample (Δz) was acquired to obtain force curves. The ramp size (vertical displacement of the piezo)

and the trigger threshold (maximum deflection of the cantilever) were set between $1.5 - 2$ µm and $300 - 400$ nm for all fibres.

The AFM height image shown in Fig. 3.4 is an example of a suspended fibre which was chosen for AFM mechanical testing. Fibres with similar orientation (approximately 45° relative to the scanning direction) were chosen for this study. The height image in Fig. 3.4 exaggerates the true diameter of the fibre due to convolution with the pyramidal AFM tip. Therefore, the diameter of each fibre was measured using the section analysis command in Nanoscope controller 8.15. Using the cross-sectional profiles, the diameter was measured at 10 different locations (5 on each side of the two supported segments) and the average and standard deviation were calculated. Fibres with more uniform cross section, i.e., lower standard deviation, were chosen for this study.
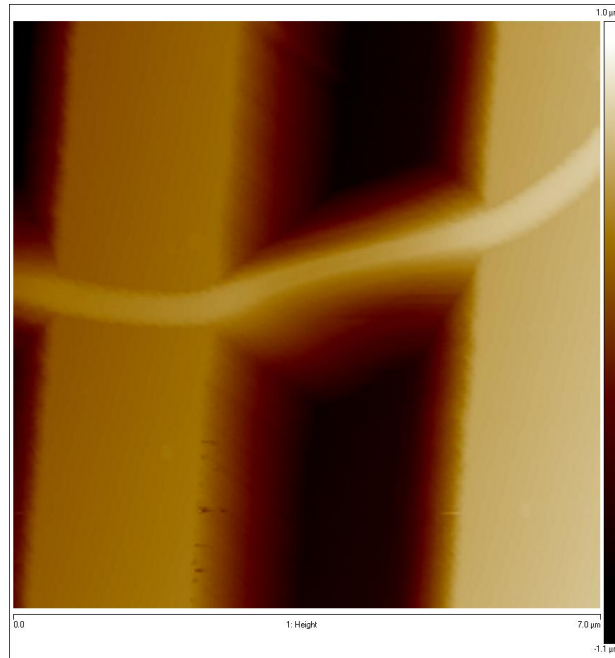
Fig. 3.4: AFM height image of a suspended PCL fibre crossing a trench

3.5.5 Contact AFM Force Plots

In contact AFM force plots, the horizontal axis demonstrates the vertical displacement of the probe relative to the sample, and the deflection of the cantilever is plotted on the vertical axis. An example of a force plot is shown in Fig. 3.5.
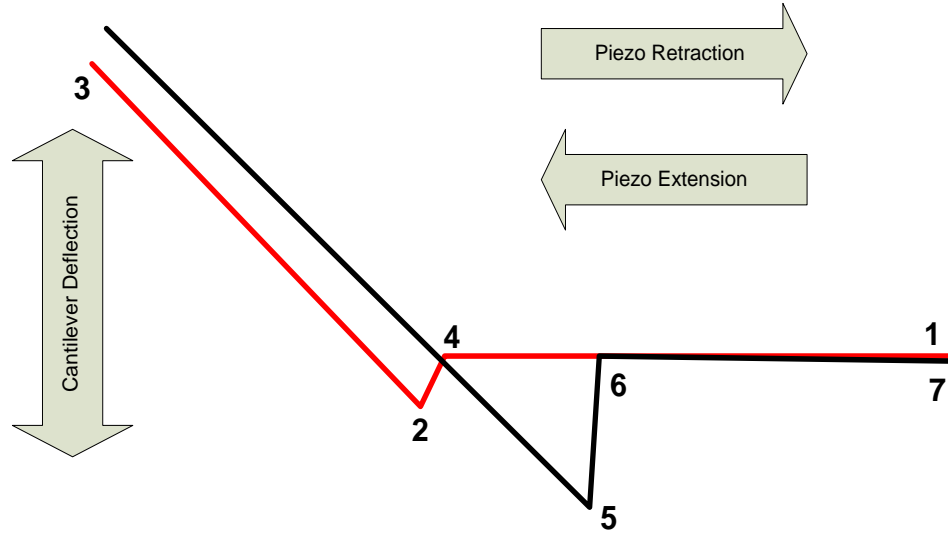
Fig. 3.5: Contact AFM force plot (adapted from [117])

Each force plot can give us significant information about sample-tip interactions. As the tip approaches the sample, it is attracted to the surface due to various forces such as electrostatic and/or surface tension (capillary forces). This can be clearly observed on the graph (Fig. 3.5) at point 2 (slight dip) where the tip suddenly plunges toward the surface during its descent. The existence of attractive forces is also evident between points 5 and 6. In this case the tip remains attached to the surface due to the attractive forces, as the piezo retracts. Fig. 3.6 and Fig. 3.7 show the step-by-step approach and retraction process respectively:
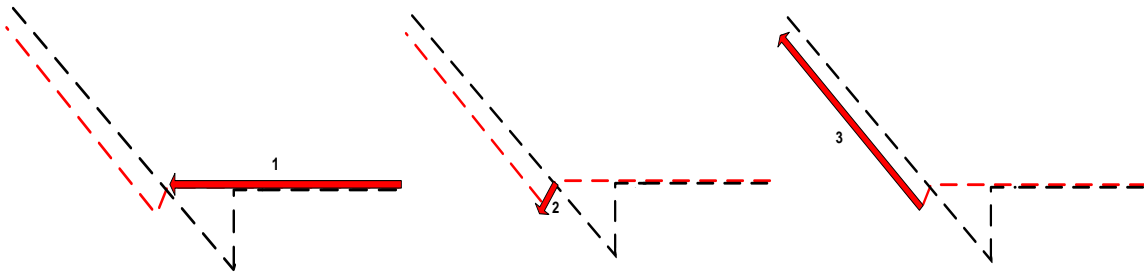
Fig. 3.6: Arrows 1-3 show the tip approach towards sample as the piezo extends

1. Piezo extends and the tip descends, however, there is no contact with the sample yet.

2. The tip is attracted to the sample by the forces near the surface.

3. The cantilever bends upward as its tip presses into the surface.

34
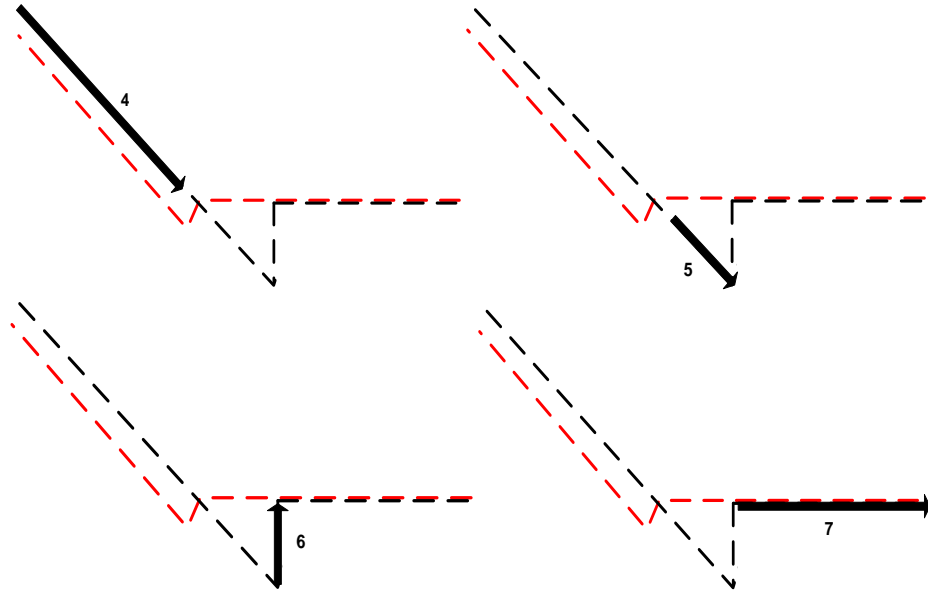
Fig. 3.7: Arrows 4-7 show the cantilever moving toward its equilibrium
position as the piezo retracts

4. Piezo retracts and this causes relaxation of the cantilever (moving downward toward its
equilibrium position) until tip forces are in equilibrium with surface forces.

5. Piezo continues retracting and the cantilever keeps bending downward. This will
continue as long as the attractive forces from the surface can keep the tip in contact with
the sample surface.

6. As the piezo retraction continues, the tip eventually breaks free of the attractive forces
and the cantilever rebounds sharply upward to its equilibrium position.

7. The tip continues moving toward its equilibrium position while the peizo continues
retracting. Hence, no further contact with the sample is seen.

Force curves reveal useful information about the elasticity of the sample material.
Cantilever deflection for a given downward tip movement is an indication of the
material's elasticity. For hard materials, the cantilever will experience larger deflections
compared with softer samples.

3.5.6 Determination of the Elastic Modulus

Force curves were acquired for multiple points along the suspended and supported part of each fibre (Fig. 3.8), and the rigid flat areas of the substrate in the vicinity of each fibre. The obtained data were then extracted from Nanoscope controller 8.15 and were analyzed using the Igor Pro software package (Wavemetrics) with a custom analysis routine. Slopes of the force plots were measured from the contact region of the approach curves and were compared with the slopes of the force curves obtained from the rigid area. On the rigid surface, the cantilever's deflection (Δy) is expected to be equal to the sample displacement (Δz).
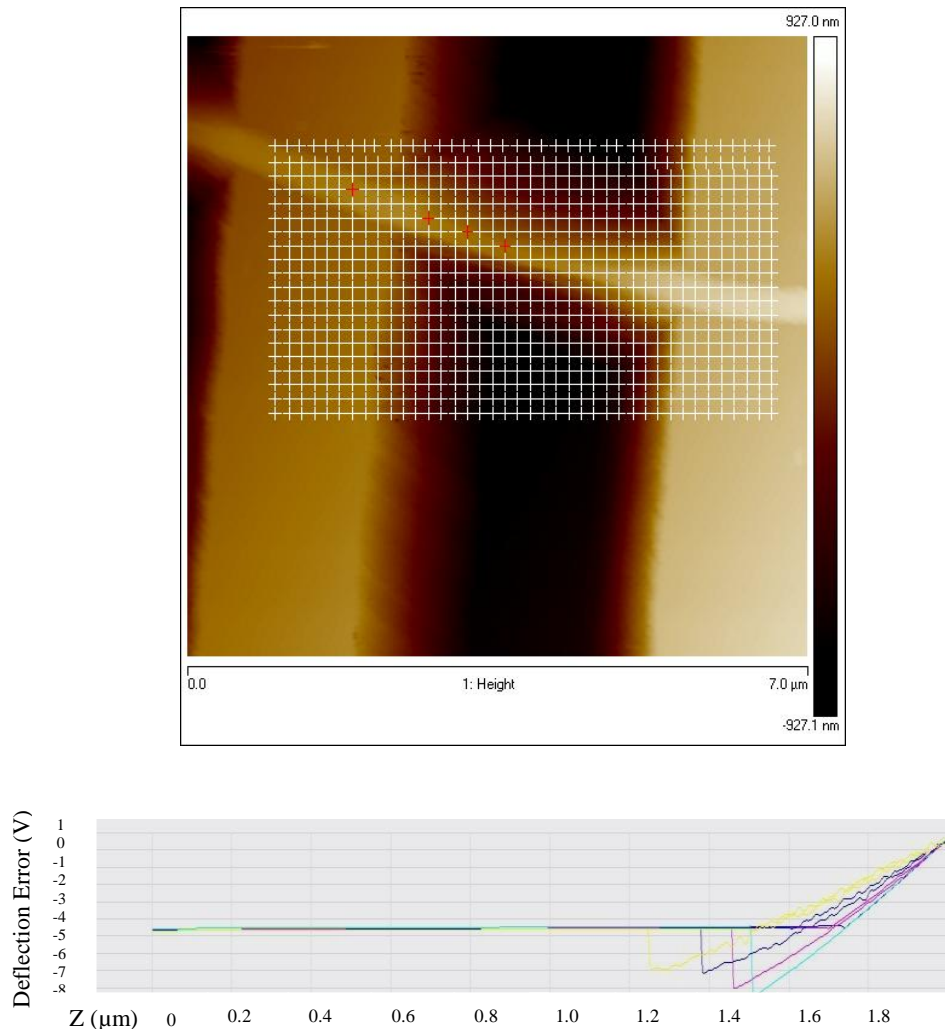
Fig. 3.8: Force curves (bottom) obtained on the supported and suspended portion of the fibre (top)

As depicted in Fig. 3.8, the slopes obtained from the rigid area and the supported segment of the fibre are steeper compared with that of the suspended portion. The theoretical slope (dy/dz) of the rigid area and the supported segment of the fibre is equal to unity which was used to calibrate the cantilever deflection's sensitivity (Δy). The calibration was performed by plotting a histogram of the slopes and normalizing the deflection signals to the mean value in the histogram.

For the suspended portion of the fibre, the total piezo displacement is greater than the deflection of the cantilever ($\Delta z > \Delta y$) because of the fibre's deformation δ (i.e., $\Delta z = \Delta y + \delta$). As a result, the slope obtained from the contact region of the force plot is less than unity (i.e., $dy/dz < 1$) for the suspended segment.

The elastic modulus was determined from the fit to more than 50 data points chosen along each fibre, from its suspended and supported portion (Fig. 3.9). The height image was used to locate the points on the fibre where the cantilever applied the force. First, 30 − 50 data points were selected on the rigid area, in the vicinity of each fibre, to measure the cantilever's deflection sensitivity. The blue points in Fig. 3.9 represent the points that were chosen for calibration of the fibre shown. The points that were chosen along the fibre to measure the fibre's deflection are shown in green. The slopes obtained from the selected force plots were plotted as a function of position a from one end of the fibre. This is demonstrated in Fig. 3.10, where the distance is measured from the onset of the fibre's suspended portion from one end.
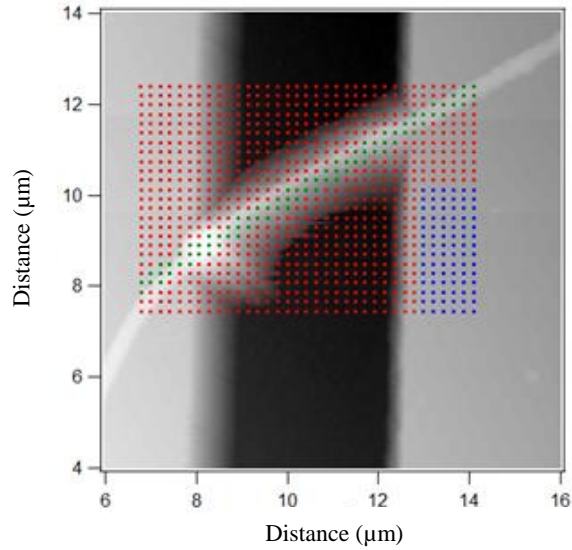
Fig. 3.9: Height image from AFM contact mode: 900 points chosen for force volume measurement, blue points were used to calibrate the cantilever's deflection sensitivity; green points were chosen along the fibre to measure fibre deflection
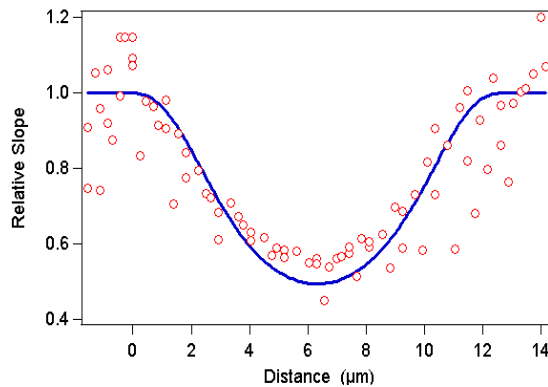
Fig. 3.10: Relative slopes of force plots, and the curve fit (blue line) obtained from multiple points along the fibre

3.6 Analytical Models

3.6.1 Pure Bending Model

The previously established clamped beam model, derived from the Euler-Bernoulli beam theory [20], was used in this study to analyze the behaviour of all PCL and collagen nanofibres. This model is based on the assumption that the supported ends of the fibre remain attached to the substrate when the force is applied.

38
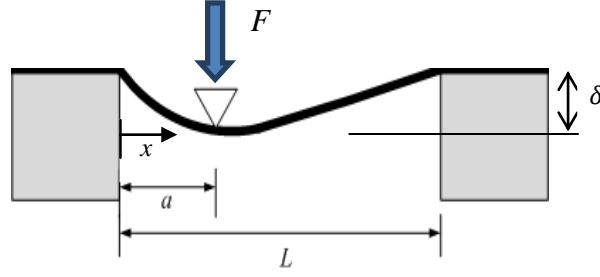
Fig. 3.11: Clamped-fibre with suspended length L deflected by δ
due to an applied force F at distance a from one end

For a suspended beam of length L subjected to a concentrated load F applied at a point along the fibre, with its location a measured relative to one end of the fibre (Fig. 3.11), the beam's deflection $\delta(x)$ can be found according to equation (3.1) [118]:

$$\delta(\mathrm{x})= \begin{cases} \frac{F}{6E_bIL^3} \left[(L + 2a)x - 3La\right](L - a)^2x^2 & 0 < x < a \\ \frac{F}{6E_bIL^3} \left[(L + 2x)a - 3Lx\right](L - x)^2a^2 & a < x < L \end{cases} \qquad (3.1)$$

where I is the area moment of inertia and E_b is the bending modulus. For a solid beam with circular cross section, the area moment of inertia can be calculated using equation (3.2):

$$I = \frac{\pi d^4}{64} \qquad (3.2)$$

where d is the fibre diameter.

In an AFM experiment, the deflection of the beam is measured at the point of contact with the cantilever where the force is exerted on the beam (i.e., $x = a$). As a result, the measured deflection is:

$$\delta(a) = \frac{F}{3E_bI} \left[\frac{a\,(L-a)}{L}\right]^3 \qquad (3.3)$$

The applied force by the cantilever is given by $F = k\,\Delta y$, where k is the spring constant of the cantilever and Δy is the deflection of the cantilever from its equilibrium position. As the piezoresistant scanner moves the sample vertically, its displacement Δz is equal to the sum of the cantilever deflection Δy and the deflection of the fibre $\delta(a)$:

39

$$\Delta z = \Delta y + \delta(a) \quad (3.4)$$

Therefore, combining equation (3.3) and (3.4) yields [21]:

$$\Delta z = \Delta y \left[1 + \frac{k}{3E_b I} \left(\frac{a(L-a)}{L} \right)^3 \right] \quad (3.5)$$

The slope of the contact portion of the force spectra is measured as:

$$\frac{dy}{dz} = \left[1 + \frac{k}{3E_b I} \left(\frac{a(L-a)}{L} \right)^3 \right]^{-1} \quad (3.6)$$

The bending modulus E_b of the fibre is the only unknown variable in equation (3.6), allowing it to be determined from a fit of the functional form of equation (3.6) to the slopes measured at a series of locations along the suspended fibre [21].

3.6.2 Deflection due to Shear

The Euler-Bernoulli model cannot capture the full behaviour of a beam's deflection, since it does not take the effect of shear into account. As a result of deflection, every section of the suspended portion of a deflected beam is subjected to shear stress. The resulting deflection due to shear can be calculated using equation (3.7) [118]:

$$\delta_{\text{shear}}(x) = \begin{cases} f_s \left(\frac{F}{GAL} \right) (L-a)x & 0 < x < a \\ f_s \left(\frac{F}{GAL} \right) (L-x)a & a < x < L \end{cases} \quad (3.7)$$

where G is the shear modulus, $A = \pi d^2/4$ is the cross-sectional area, and f_s (10/9 to 7/6) is a numerical factor which depends on the Poisson's ratio for the material. Timoshenko's beam theory provides a more accurate bending model by considering the

deflection due to shear. Using Timoshenko's model, the ratio of the deflection vs. the applied force ($\frac{\delta}{F}$) as a function of position along a suspended fibre is [119, 118]:

$$\frac{d\delta}{dF} = \frac{64}{3\pi d^4}\left[\frac{a(L-a)}{L}\right]^3 e + \frac{4f_s}{\pi d^2}\frac{a(L-a)}{L}g \qquad (3.8)$$

where $e = 1/E$ and $g = 1/G$. Using $a = L/2$ in equation (3.8), and rearranging for E (Young's modulus) results:

$$E = \frac{L^3}{3\pi d^4}\frac{1}{\frac{d\delta}{dF}|_{a=L/2}}\left(1 + \frac{3f_s}{\pi}\frac{d^2}{L^2}\frac{E}{G}\right) \qquad (3.9)$$

By rearranging equation (3.3), and using $a = L/2$ we define the bending modulus as:

$$E_b = \frac{L^3}{3\pi d^4}\frac{1}{\frac{d\delta}{dF}|_{a=L/2}} \qquad (3.10)$$

Using equation (3.10), equation (3.9) can be rewritten as:

$$E = E_b\left(1 + \frac{3f_s}{\pi}\frac{d^2}{L^2}\frac{E}{G}\right) \qquad (3.11)$$

3.6.3 Deflection due to Tension

The Euler-Bernoulli and Timoshenko beam theories are based on the assumption that the length of a suspended beam does not change during bending. However, in reality, the beam stretches due to deformation which in turn induces an inherent axial tensile force. Heidelberg *et al.* demonstrated that the tensile stress should be taken into account when the fibre experiences significant lateral displacement (i.e., displacement much greater than fibre's radius) [109]. Heidelberg *et al.*'s mathematical model which was used in this study to investigate the effect of tensile forces on the fibres' elasticity is included in Appendix A.

Chapter 4: Results

4.1 Young's Modulus of PCL

In this study, the Young's modulus of electrospun poly(caprolactone) (PCL) nanofibres was investigated using four different bending models. First, the Euler-Bernoulli beam theory was used based on the assumption that the fibres experienced "pure bending" and the inherent shear stress and tensile forces had negligible effect on fibres' bending behaviour. To test the validity of this assumption, the Timoshenko beam model was applied to investigate the influence of shear. Finally, the models due to Heidelberg *et al.* and Hudson *et al.* were used to examine the effect of axial tensile forces induced as a result of stretching, and the effect of any initial tension due to the pre-existing strain in the fibres, respectively.

4.1.1 The Euler-Bernoulli Model

Equation (3.6) in chapter 3 was used to determine the Young's modulus of PCL fibres according to the Euler-Bernoulli beam theory. For each fibre, the Young's modulus was obtained from a fit to the relative slopes of force curves (i.e., plots of deflection vs. piezo position) obtained from multiple points along each fibre. Fig. 4.1.a shows the Young's modulus thus determined of 64 PCL fibres with diameters in the range of 88 - 409 nm. A sharp increase can be seen for the Young's modulus as the fibre diameter is decreased. Moreover, as shown in Fig. 4.1.b, Young's modulus increases drastically as the aspect ratio (d/L) is decreased. Since there is a dependence on aspect ratio predicted by the Timoshenko theory, further investigation is required in order to determine whether the contribution of shear stress was significant.
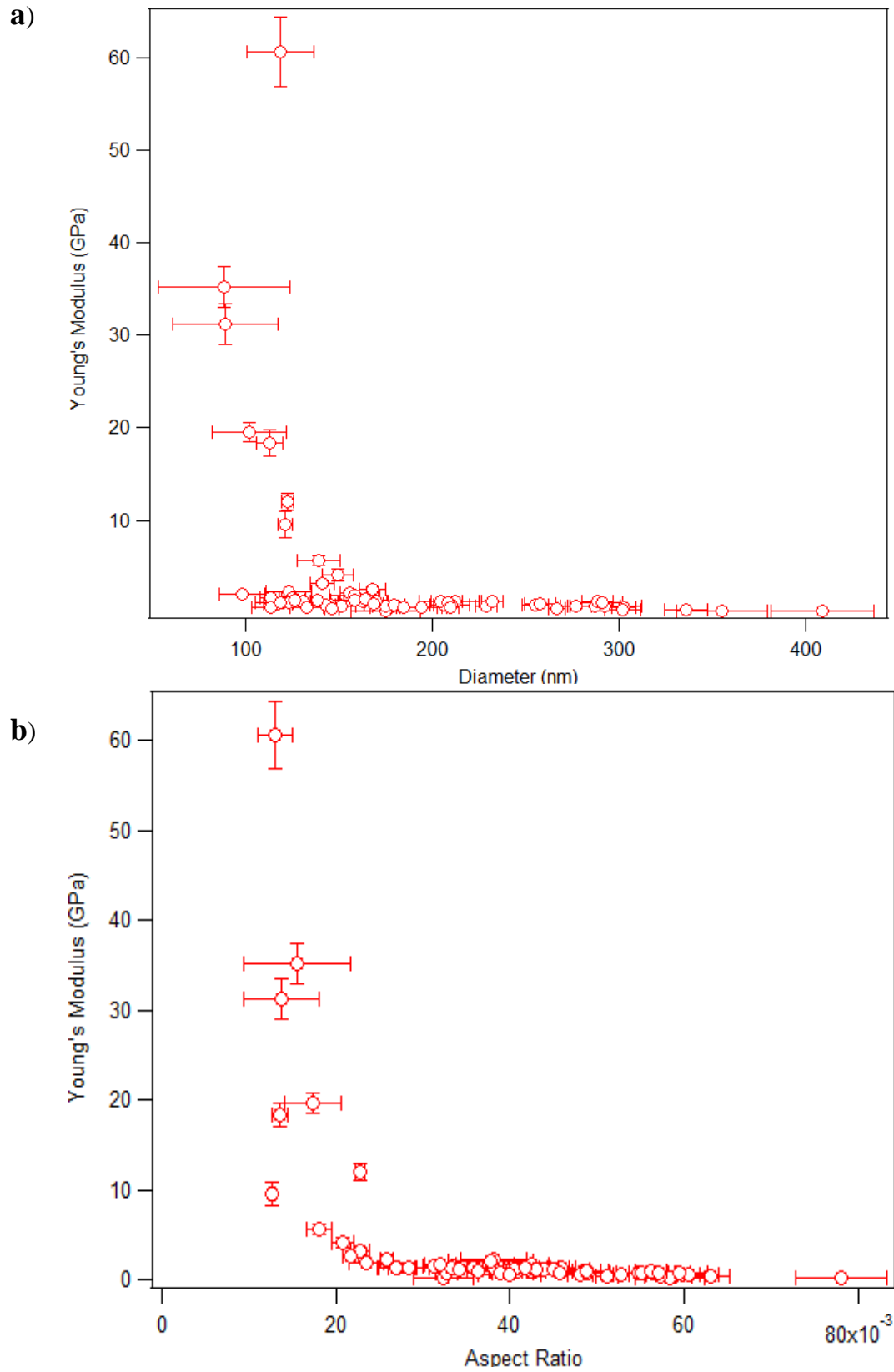
Fig. 4.1: Young's modulus vs. a) diameter and b) aspect ratio for PCL fibres

43

Individual plots of relative slopes vs. position were carefully examined for each fibre in order to verify whether the pure bending model was satisfactory. It was observed that for many fibres, independent of their diameter, the curve fit did not match the data for the plot of relative slopes vs. distance. As is shown in Fig. 4.2.a, obtained from a fibre with d ~ 145 nm, the curve fit can represent the bending behaviour of the fibre. In contrast, in Fig. 4.2.b, the fit is clearly not a good representation of the data for a fibre with d ~ 89 nm. It is evident from Fig. 4.2.b that the pure bending model of the Euler-Bernoulli is not adequate to demonstrate the true bending behaviour of the fibre. A more complete analysis of the bending results is described in Section 4.1.2 using Timoshenko's beam theory.
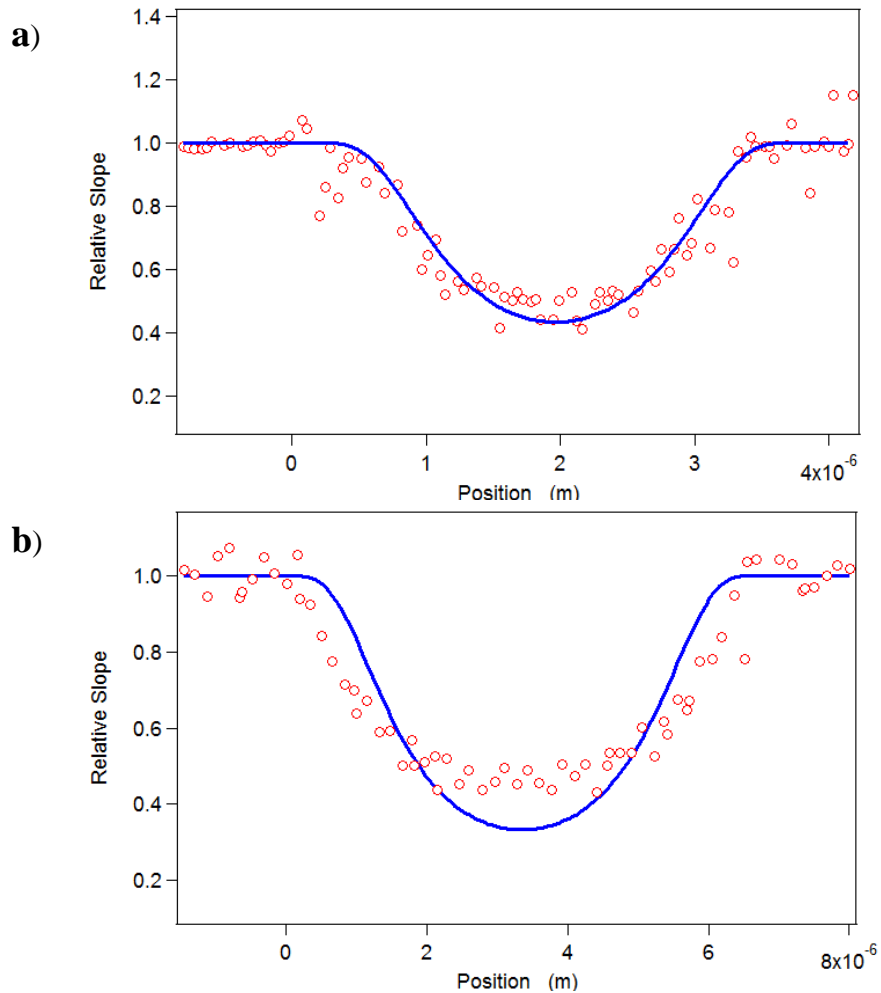
Fig. 4.2: Plot of relative slopes vs. position for PCL fibres with a) d ~ 145 nm, b) d ~ 89 nm

4.1.2 Timoshenko's Model

In the Euler-Bernoulli model, it is assumed that the restoring force is only due to the compressive and tensile stresses along the axis of the beam as a result of "pure bending" and the internal shear stress is negligible [20]. However, we were unable to obtain valid results for the Young's modulus of PCL fibres by using this assumption. This might be due to the fact that in reality, every section of a deflected beam is subjected to shear stress. The effects of shear can be accounted for by adding a second term to the Euler-Bernoulli equation for beam deflection, as was previously established by Timoshenko [118]. Therefore, in order to take the shear effects into account, Timoshenko's beam theory was applied to investigate the deflection of PCL fibres as a result of both bending and shear. Using equation (3.8) in Chapter 3, a new fit was obtained for the data points in the plots of relative slopes vs. position. As is evident in Fig. 4.3, the new curve fit is a better representation of the data.
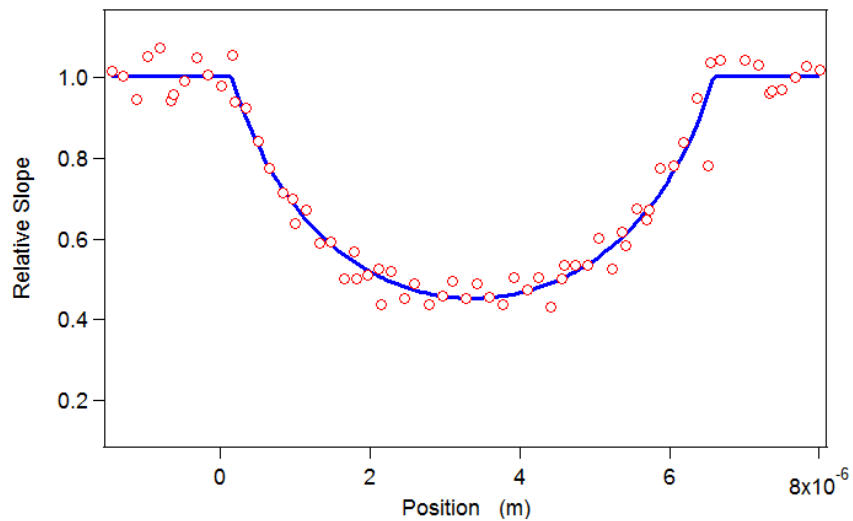
Fig. 4.3: Relative slopes and the curve fit (blue line) for PCL fibre of $d \sim 89$ nm

Furthermore, using equation (3.8) E and G were calculated for each PCL fibre. However, due to the strong covariance between the two parameters of interest, definitive values could not be calculated for E and G, since by increasing E and decreasing G, or vice versa, a satisfactory fit could be obtained. However, Timoshenko has a prediction model for the dependence of bending modulus on aspect ratio (equation (3.11) in Chapter 3):

$$E_b = E/(1 + \frac{3f_s}{\pi} \frac{d^2}{L^2} \frac{E}{G})$$

45

where E_b is defined as the Young's modulus that would produce the observed minimum slope in a fibre for which bending alone (and not shear) is important. The bending modulus and Young's modulus are therefore the same if shear can be neglected; otherwise the bending modulus is smaller than the Young's modulus. This model was used to verify the validity of the Timoshenko model for the data obtained for PCL fibres. It is evident that the bending modulus and the Young's modulus become equal as d/L approaches zero. As a result, the effect of shear is expected to be more significant on fibres with larger aspect ratio.

Similar to Fig. 4.1.a, Fig. 4.4.a demonstrates a decreasing trend for bending modulus vs. diameter. The bending modulus was estimated using the fibres' deflection at $L/2$, which was calculated using the minimum relative slope from the curve fits obtained from Timoshenko's model. This minimum relative slope allowed us to get an estimate of the "bending modulus" at the centre of the fibre. There is a clear prediction of how the bending modulus should depend on the aspect ratio of the fibre. As is evident from Fig. 4.4.b, by applying the predicted model we have obtained a fit which is satisfactory only for large aspect ratios. However, this prediction yields an unreasonably large Young's modulus of several hundred TPa. Therefore, shear effects cannot account for the observed increase in the bending modulus at small diameters.

a)

b)

Coefficient values ± one standard deviation
young   =6.4697e+14 ± 2.71e+14
shear   =6.9258e+06 ± 1.61e+05
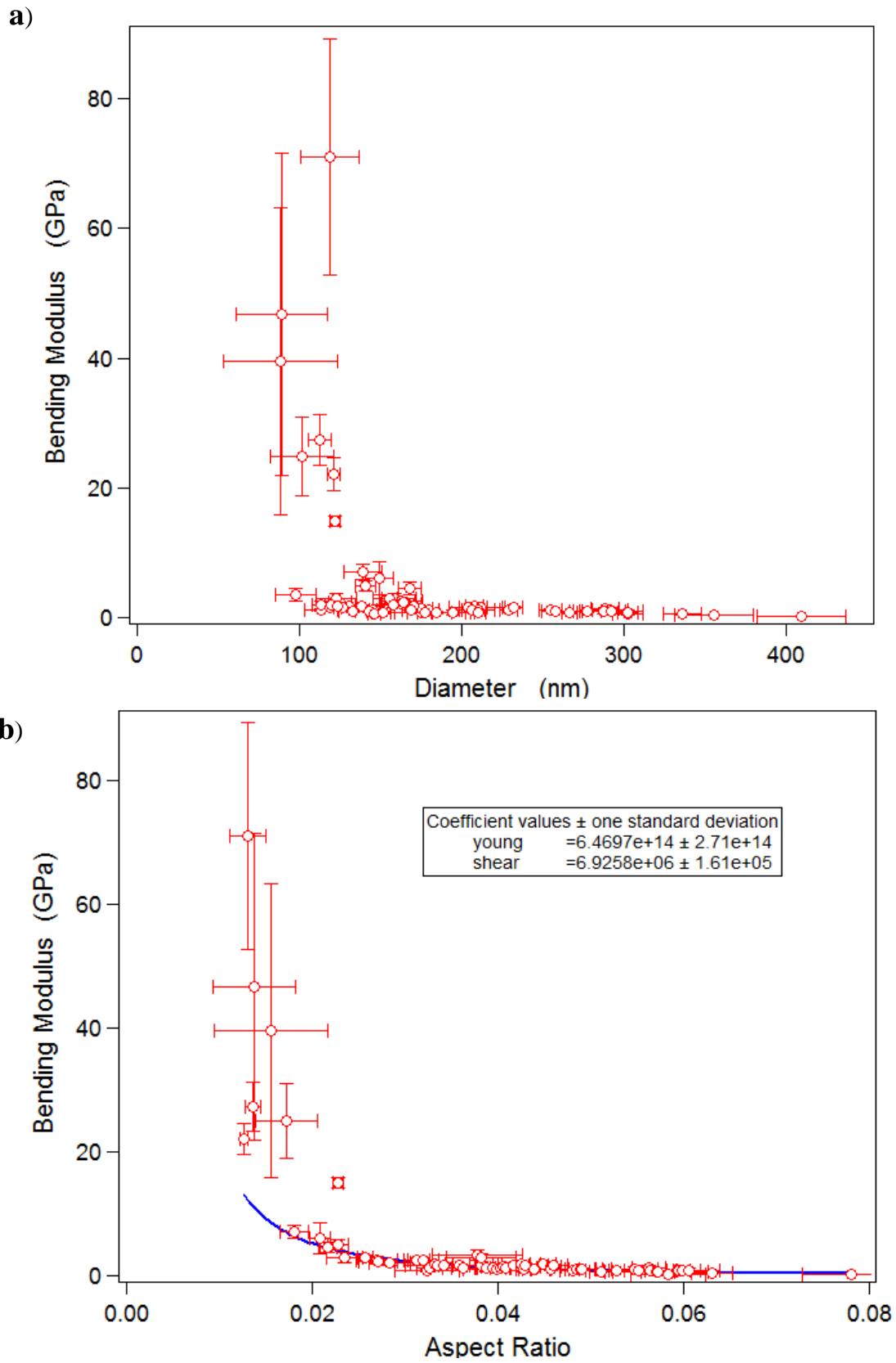
Fig. 4.4: Bending modulus vs. a) diameter, b) aspect ratio for PCL Fibres

However, it was observed that the force curves (i.e., plots of cantilever deflection vs. piezo position) were non-linear (in the contact region) for many fibres, independent of their diameter. Examples of linear and non-linear force curves are depicted in Fig. 4.5.a and Fig. 4.5.b, respectively. Due to the nonlinearity of the contact region in Fig. 4.5.b, an arbitrary and inaccurate slope is captured. As a result, it can be concluded that the pure bending model of Euler-Bernoulli cannot capture the actual bending behaviour of all fibres, and the validity of the increasing trend for the Young's modulus observed in Fig. 4.1 and Fig. 4.4 needs further investigation using more sophisticated beam theories.
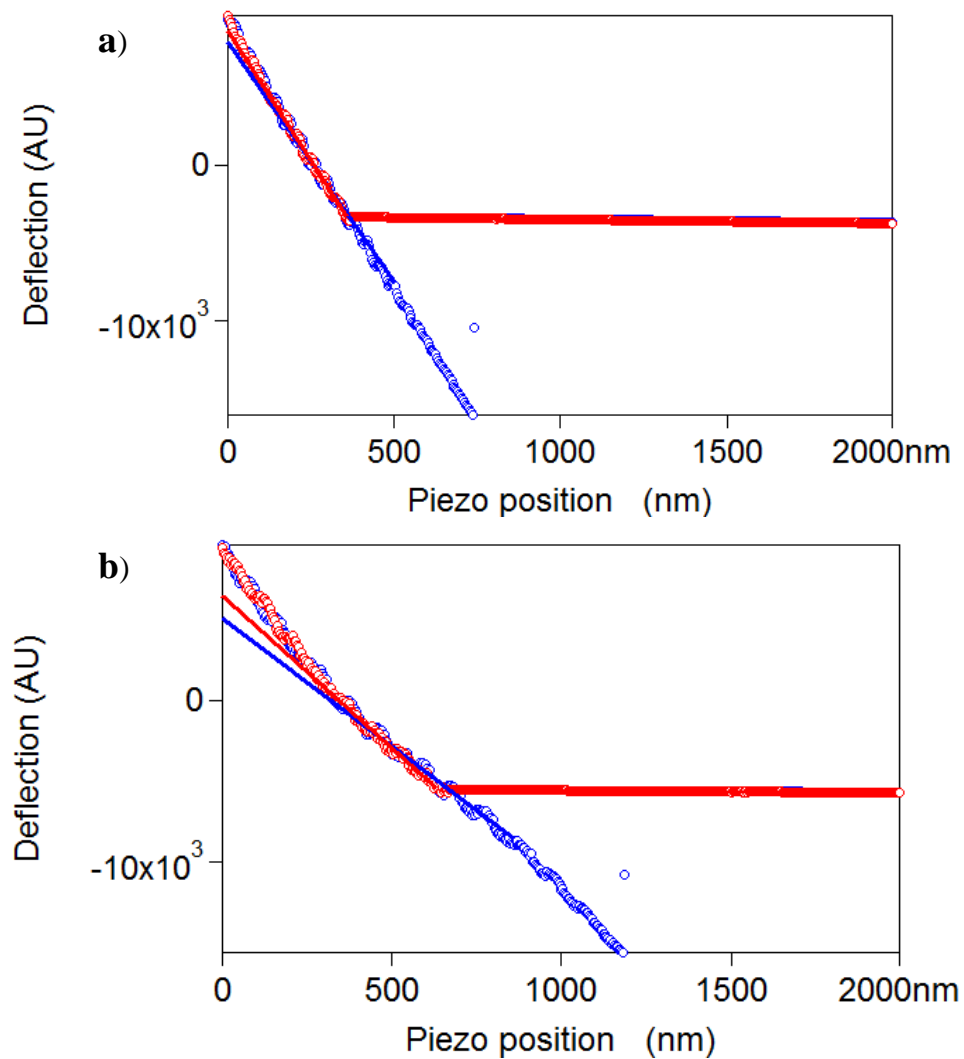
Fig. 4.5: Deflection vs. piezo position for a PCL fibre with a) $d \sim 1.45$ nm, b) $d \sim 89$ nm

4.1.3 Models of Heidelberg *et al.* & Hudson *et al.*

As demonstrated in previous sections, the Euler-Bernoulli pure bending model and Timoshenko's shear model could not capture the actual behaviour of PCL fibres. Implicit in both these models is the assumption that the deflections were small enough that the fibre's elongation due to stretch was negligible, and the length of the fibre could be considered constant during bending. This may not be a good approximation for small diameters, where resistance to stretching might be as important as resistance to bending. Moreover, it was assumed that there was no pre-existing strain in the fibres. The influence of tension was previously addressed by Heidelberg *et al.* and Hudson *et al.* who applied more complex models to examine whether the effect of tension could account for the observed response of narrow fibres [109, 120]. These models are more complicated than the previous models and we only attempted to apply them to a few force curves near the centre of each fibre, rather than to the entire profile of force curves. As demonstrated through equations (A.4) to (A.6) in Appendix A, the function $f(\alpha)$ represents the increase in the fibre's resistance to deformation due to the increase in tensile stress accompanying the deformation of the fibre. This factor was not previously taken into account in the Euler-Bernoulli model, where only bending stress was assumed to be significant. Heidelberg *et al.*'s system of equations, (A.4) to (A.8) in Appendix A, were applied to the multi-point bending results of PCL fibres, with the Young's modulus as the sole free parameter. Force vs. fibre deflection curves were plotted for a few points near the centre of the fibre using the information which was acquired from the force curves: cantilever's deflection Δy (i.e., $\Delta y = F/k$) and fibre's deformation δ (i.e., $\delta = \Delta z - \Delta y$). Fits to the entire range of data could only be obtained for fibres that experienced elastic deformation (i.e., the yield point was not reached). Fig. 4.6.a shows an example of a force vs. deflection curve for a fibre which was not deformed beyond its elastic limit. In contrast, in Fig. 4.6.b, the fibre had reached its yield point and had undergone plastic deformation.
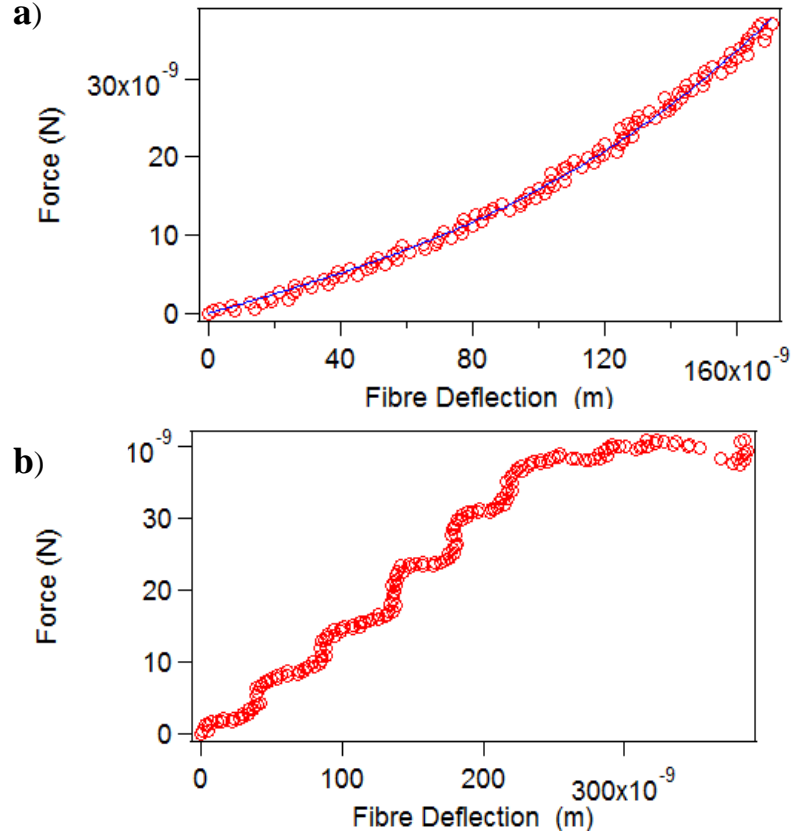
Fig. 4.6: Force vs. fibre deflection for:
a) fibre deformation in the elastic range, b) fibre reaching its elastic limit

Hudson *et al.*'s system of equations, (A.4), (A.5), and (A.14) in Appendix A, were also applied to obtain the Young's modulus from the fit to force vs. displacement data, with the initial tension and Young's modulus as free parameters. However, it should be noted that Heidelberg *et al.* and Hudson *et al.*'s models were developed only for loads applied at the centre of the fibre. As a result, we used a few points approximately located around the centre (i.e., at $L/2$) for the purpose of this analysis, and calculated the average value. A key feature of Heidelberg *et al.* and Hudson *et al.*'s model is that it can explain the curvature which was observed in the contact region of the plots of deflection vs. piezo position. In contrast, both Euler-Bernoulli and Timoshenko's models predict a linear contact region.

Fig. 4.7 is a plot of Young's modulus vs. diameter, as determined using Heidelberg *et al.*'s model. It can be seen in Fig. 4.7 that the obtained data is scattered and does not show a clear dependence on diameter (for $100 \leq d \leq 400$ nm). By applying an extension of Heidelberg *et al.*'s model, previously established by Hudson *et al.*, the Young's modulus was recalculated by considering the possibility of pre-existing tension in fibres. An initial tension in fibres might be expected due to the violent nature of the electrospinning fabrication process (i.e., fibre deposition and immediate solvent evaporation). As is evident in Fig. 4.8, the Young's modulus does not show any dependence on diameter for PCL fibres of approximately $100 - 400$ nm in diameter. Furthermore, comparison of Figs. 4.7 and 4.8 reveals that initial tension had a greater impact on narrow fibres compared with those of larger diameter. In other words, the results indicate that initial tension is more important for narrow fibres.
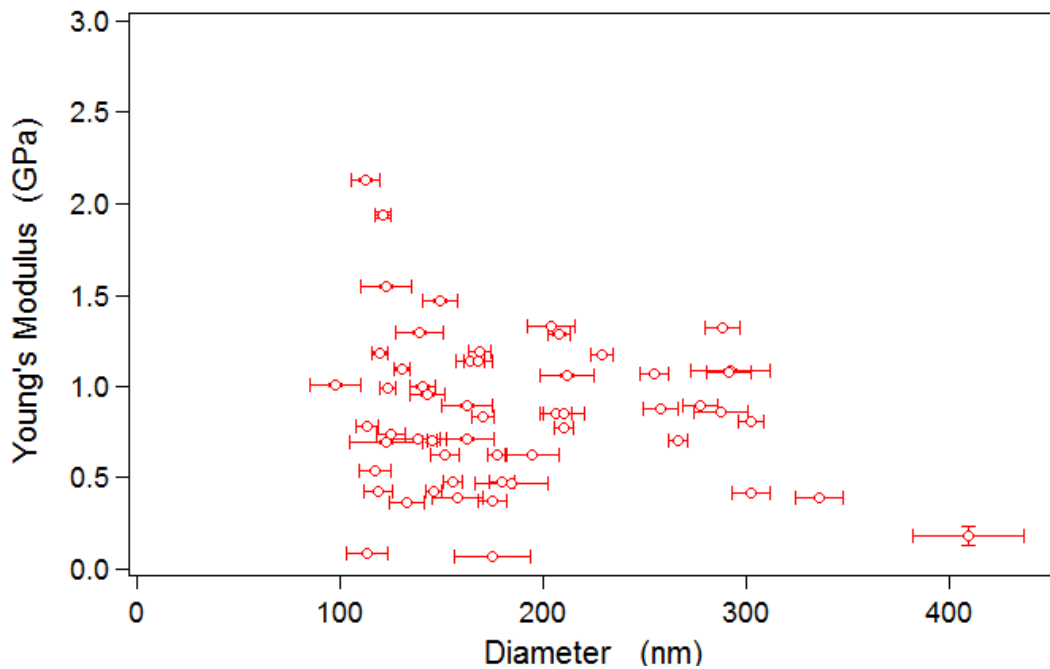
Fig. 4.7: Plot of Young's modulus vs. diameter for PCL fibres - axial tension due to fibres' elongation is taken into account using Heidelberg *et al.*'s model

51
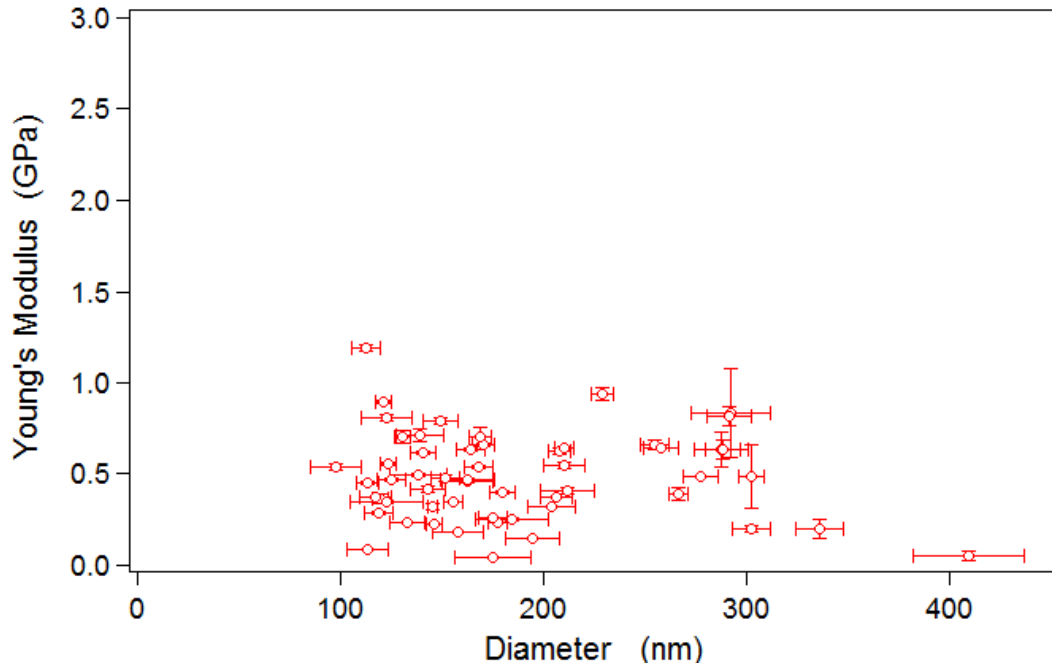
Fig. 4.8: Plot of Young's modulus vs. diameter for PCL fibres - initial tension and the tension due to elongation are taken into account using Hudson *et al.*'s models

The Gaussian distribution of the moduli obtained from Hudson *et al.*'s model is presented in Fig. 4.9, indicating an approximate Young's modulus of 0.5 GPa. Analyzing the results using Heidelberg *et al.* and Hudson *et al.*'s models eliminated the apparent increase in Young's modulus at small diameters, with the exception of a few fibres with diameters of approximately 100 nm. This strongly suggests that much of the increasing trend observed in Fig.4.1 and Fig.4.4 for the modulus was an artefact of not considering the overall stretching that accompanies bending of the fibre. Heidelberg *et al.* have demonstrated that this stretching effect must be taken into account when the lateral displacement of the fibre is comparable to or larger than the fibre's radius [109]. In principle, the model of Heidelberg *et al.* will produce the same result as the Euler-Bernoulli model in the limit of small deflections or large aspect ratios, assuming that the initial tension is negligible. Comparison of Fig. 4.7 with Fig. 4.4.a and Fig. 4.1 demonstrates that the PCL fibres in this study had experienced enough displacement that the effect of axial tensile forces could not be ignored. Moreover, comparison of Fig. 4.7 with Fig. 4.8 shows that considering the pre-existing tension results in a further decrease in the calculated

modulus. However, the effect of tensile forces and the pre-existing tension is less significant on fibres with larger diameter.
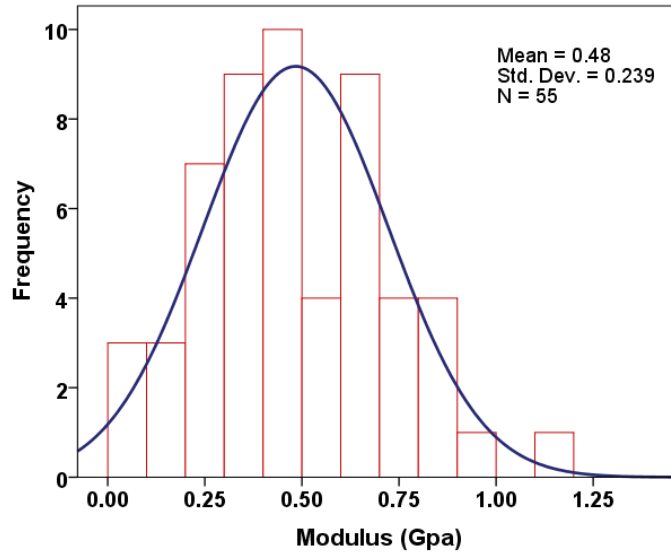
Fig. 4.9: Gaussian distribution of the Young's moduli of PCL fibres obtained from Hudson *et al.*'s model

4.2 Young's Modulus of Collagen Fibres

For tissue engineering applications, it is essential that the mechanical properties of the artificial scaffold mimic those of the native extracellular matrix [8]. Therefore, in order to compare the Young's modulus of PCL fibres with that of collagen, collagen type I electrospun fibres from rat tail were collected for multi-point bending tests. Also, another batch of collagen fibres was cross-linked with genipin, in order to compare the Young's modulus of as-spun and stabilized collagen fibres for cell-culture applications.

In this study, we investigated the Young's moduli of as-spun and cross-linked collagen fibres using an approach similar to that described in Section 4.1 for PCL fibres. First, the Young's moduli were determined using the Euler-Bernoulli model, assuming that shear and tensile stresses were negligible. Fig. 4.10 shows the Young's moduli of 14 as-spun and 10 cross-linked collagen fibres, as obtained from the pure bending model. It can be seen that the Young's modulus is increased as the fibre diameter is decreased for both as-spun and cross-linked collagen fibres.
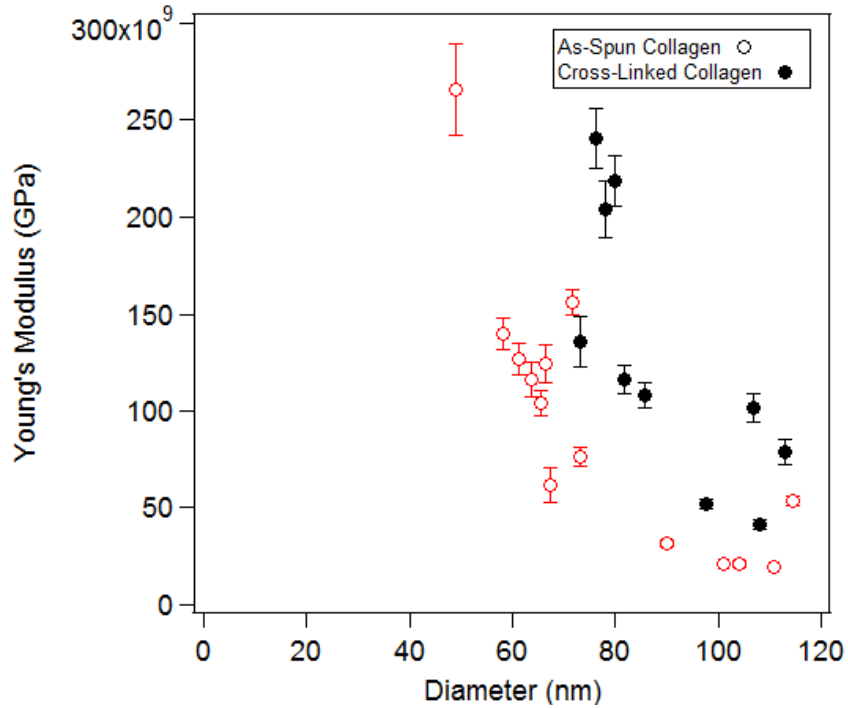
Fig. 4.10: Young's modulus vs. diameter for as-spun vs. cross-linked collagen nanofibres obtained from the Euler-Bernoulli model

Applying the Euler-Bernoulli model resulted in unreasonably large modlui for as-spun and genipin-cross-linked collagen fibres. Therefore, the Young's moduli were also obtained from Hudson *et al.*'s model to investigate the effect of tension. These results are presented in Fig. 4.11 for both as-spun and cross-linked collagen fibres. As is evident in Fig. 4.11, the obtained results for the Young's moduli have significantly decreased in value and are more constant compared with those of the Euler-Bernoulli model. This is similar to the results obtained for PCL fibres in Section 4.1, and is indicative of the effect of tensile forces and possible pre-existing strain on fibres' deflection. The presence of initial tension was anticipated for as-spun and cross-linked collagen fibres, since collagen fibres were fabricated using the electrospinning technique and were subjected to immediate solvent evaporation and violent deposition on substrate during sample collection.
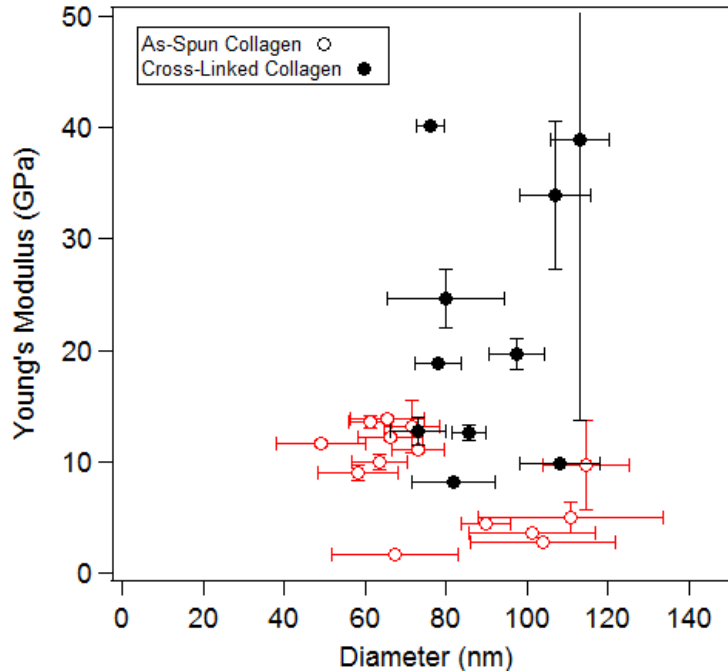
Fig. 4.11: Young's modulus vs. diameter for
as-spun vs. cross-linked collagen nanofibres obtained from Hudson *et al.*'s model

Heidelberg *et al.*'s model was also used to analyze the force curves obtained from multi-point bending tests. However, the resulting fits to data were not satisfactory for the majority of the fibres, indicating that Heidelberg *et al.*'s assumption of zero initial tension is not valid for the electrospun fibres examined in this study.

The box plot in Fig. 4.12 summarizes the results of as-spun and cross-linked collagen fibres obtained from Hudson *et al.*'s model. The Young's modulus of as-spun and cross-linked collagen fibres were determined with a range of 1.66 – 13.9 GPa and 8.22 – 40.1 GPa, respectively, indicating that cross-linked collagen fibres have a higher stiffness compared with as-spun collagen fibres. The significance of these results from the tissue engineering perspective is discussed in Chapter 5.
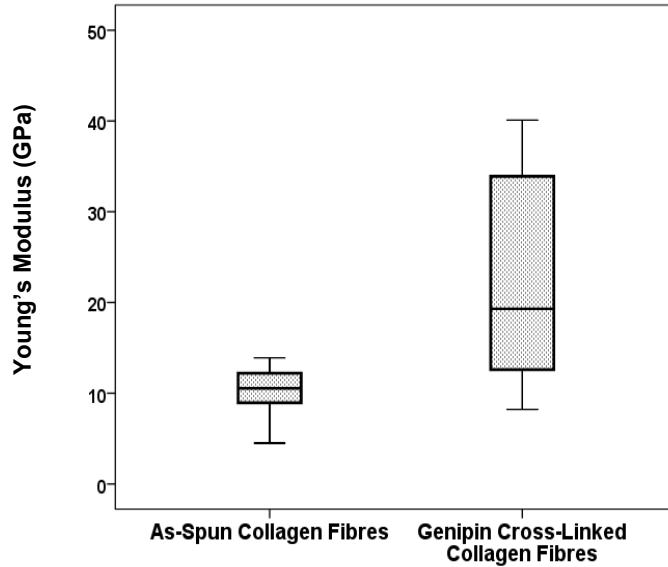
Fig. 4.12: Young's moduli for as-spun and cross-linked collagen fibres

4.3 Preliminary Results for Core-Shell Fibres

For tissue engineering applications, proteins, growth factors or drugs must be incorporated into electrospun fibres to promote cell growth and tissue regeneration. As a result, the mechanical properties of hollow and core-shell fibres must also be examined and verified to be compatible with those of collagen fibres in the native extracellular matrix. To achieve this goal, core-shell fibres were fabricated using the custom-designed coaxial electrospinning set-up described in Chapter 3. Hollow and core-shell PCL and collagen electrospun fibres were collected on TEM grids for transmission electron microscopy (TEM). Also, PCL fibres loaded with bovine serum albumin-fluorescein isothiocyanate (BSA-FITC) were collected on glass for confocal imaging. Examples of TEM images obtained from core-shell electrospun PCL and collagen fibres are included in Appendix B and Appendix C, respectively. An example of a laser scanning confocal microscopy (LSCM) image for PCL fibres loaded with BSA-FITC is included in Appendix D.

As is evident in the TEM images, both solid and core-shell fibres were found in a batch of fibres collected from coaxial electrospinning, for both collagen and PCL samples. Moreover, core-shell fibres did not have consistent inner and outer diameter size. It can

be observed that in many fibres, the thickness of the shell varied throughout the fibre. As a result, definitive results of the average inner and outer diameters could not be obtained. These preliminary results suggest that there is a need to optimize the coaxial electrospinning process in order to increase the yield of core-shell/hollow fibres with less variability in the size and shape of the core and shell structure. This is because the inner and outer diameter of a core-shell/hollow fibre must be determined precisely in order to analyze the results of multi-point bending tests, and this requires a consistent batch of fibres.

Chapter 5: Discussion

5.1 Overview

The aim of this study was to investigate the potential application of poly(caprolactone) (PCL) and collagen nanofibrous scaffolds for tissue engineering of the tympanic membrane.

PCL and collagen are biocompatible and biodegradable polymers which have been utilized to fabricate various tissue engineering scaffolds [12, 14]. PCL is a synthetic polyester and has several FDA-approved biomedical applications [10], since after degradation its by-products are neutral and do not alter the pH of the local tissue environment [11]. Moreover, PCL is hydrophobic, and therefore degrades at a relatively slow rate in aqueous solutions which can be beneficial for certain tissue engineering applications. On the other hand, collagen is considered as one of the most ideal biopolymers for tissue engineering scaffolds due to its unique mechanical properties and being one of the most abundant proteins in the extracellular matrix (ECM) [14]. However, collagen fibres are hydrophilic and degrade at a relatively higher rate compared with PCL fibres. Moreover, collagen fibres fabricated by the electrospinning process do not possess the structure of the natural collagen fibres and therefore are unstable in aqueous solutions including cell culture media. As a result, they must be stabilized using a cross-linking agent before they can be applied in cell culture applications. This can be regarded as an advantage as the degradation rate of these fibres can be tuned by controlling the detailed conditions of the cross-linking reaction [121].

Both microporous and nanofibrous scaffolds have been developed and investigated for tissue engineering applications. However, the nanofibrous structure is believed to better mimic the abundance of protein fibres and the 3D environment of the native extracellular matrix [13]. Recent studies on the structure of the tympanic membrane with high resolution microscopy reveal the abundance of well organized collagen fibres with individual fibre diameters in the range of 20 – 50 nm.

Electrospinning is becoming one of the most popular methods to prepare such scaffolds due to its versatility and ease of use. Scaffolds created using electrospinning show high surface area to volume ratio, high porosity, and high pore interconnectivity which are essential for cell adhesion, migration, and proliferation [13].

In addition, the stiffness of a tissue engineering scaffold must be compatible with that of the structural components of the native extracellular matrix, since cells can feel and respond to the stiffness of the substrate to which they are attached [8] . Therefore, for tissue engineering of the tympanic membrane, it is necessary to determine the stiffness of individual fibres of the electrospun fibrous scaffolds. In this study, the Young's moduli of electrospun PCL nanofibres as well as that of the as-spun and genipin-cross-linked collagen nanofibres were investigated.

To date, numerous studies have been conducted on the mechanical properties of various polymeric nanofibres. Several investigators have reported a possible correlation between mechanical properties and diameter of nanofibres, claiming that the mechanical properties are significantly enhanced as the diameter is decreased [122, 107, 123]. Several nanomechanical characterization techniques have been developed and reported in the literature to determine the stiffness of nanofibres [95]. The three-point bending technique based on the atomic force microscope (AFM) has recently seen an increasing interest due to its subnanonewton sensitivity. Several mechanical models of increasing level of complexity have been developed to explain the observations and to determine the Young's modulus of nanofibres [109, 21, 119]. These models have been applied to the experimental data as demonstrated in Chapter 4.

5.2 Young's Modulus of PCL Fibres

In this study, multi-point bending test with an atomic force microscope (AFM) was used to determine the Young's modulus of electrospun PCL fibres. The data were analyzed using four different models as was described in Chapter 3 and 4. It was demonstrated that inaccurate assumptions and inadequate analytical models which do not capture the full bending behaviour of fibres may lead to arbitrary and inaccurate Young's modulus

determination. As shown in Chapter 4, an increasing trend was observed for PCL fibres when the effect of shear and tensile forces were not taken into account. However, consistent results were obtained when more complete models (i.e., those of Heidelberg *et al*. and Hudson *et al*.) were used to take into account the effect of induced tensile forces due to stretching and initial tension. The average Young's modulus obtained using Hudson *et al*.'s model is consistent with the bulk modulus of PCL (250 – 430 MPa) reported in the literature [91]. This suggests the importance of using a model which accounts for the induced tension due to elongation and the possibility of pre-existing strain in the fiber.

5.2.1 Related Studies using AFM Bending Test

In a similar study, recently conducted by Croisier *et al.*, mechanical properties of individual PCL fibres ranging from 250 to 700 nm were investigated using an AFM-based three-point bending method [124]. The fibres were electrospun using a 15 wt% PCL (Mn 80,000) polymer solution, and a similar approach was used to determine the Young's modulus using deflection vs. pizeo displacements recorded for multiple points along suspended fibres. Croisier *et al*. assumed that there was no shear contribution in the deflection of fibres. Croisier *et al*. reported a Young's modulus of 3.7 ± 0.7 GPa for single PCL fibres of 250 - 700 nm in diameter [124]. They also reported that they did not observe any dependence on diameter, which is consistent with the results presented in this study. However, the Young's modulus of 3.7 ± 0.7 GPa is significantly higher than the modulus of PCL bulk material. Croisier *et al*. did not consider the possible effect of axial tension due to the elongation of fibres during bending, and the possible pre-existing tension due to electrospinning. However, we have demonstrated that ignoring the effect of axial tension in the fiber can lead to inaccurate and arbitrary results from AFM bending measurements.

Similar studies have been conducted on other polymeric nanofibres as well as nanowires [107, 106, 109, 125]. In a study conducted by Bellan *et al.*, the Young's modulus of polyethylene oxide (PEO) nanofibres was reported to be significantly higher than that of the PEO bulk material, although no correlation between the Young's modulus and

diameter was found [107]. Bellan *et al.* attributed the increase of PEO nanofibres' elastic modulus to the molecular alignment of PEO chains in the fibres [107]. The authors reported that residual tension in fibres was assumed to be negligible; however they did not justify this assumption. In another study, Cheng *et al.* used the AFM-based three point bending method to investigate the elastic modulus of cellulose fibrils [106]. A Young's modulus of 93 GPa was determined for Lyocell fibrils with d ~ 170 nm which is significantly higher than that of Lyocell fibres (11-13 GPa for $d = 12.64 \pm 1.15$ μm) from which the fibrils were isolated [126, 106].

In this study, we have demonstrated that multi-point bending test on PCL and collagen nanofibres could yield an overestimated result of the actual elastic moduli if the effect of axial tensile forces due to elongation of the fibres, and the residual tension is not taken into account. Heidelberg *et al.* and Wen *et al.* also demonstrated that for Si and ZnO nanowires, the induced axial tensile forces could fully explain the apparent increase in Young's modulus at small diameters, and the moduli were found to be identical to that of the bulk value for both Si and ZnO [125, 109].

5.2.2 Other Studies on PCL

In a recent study conducted by Wong *et al.*, the effect of fibre diameter on tensile properties of electrospun PCL ($M_w = 80,000$) fibres was investigated using an ultra-sensitive Instron (MTS NanoBionix) [123]. The tensile testing results indicate that the Young's modulus increased approximately from 220 to 350 MPa when the diameter was reduced from 2.5 μm to 250 nm [123] . Also, wide angle x-ray diffraction (WAXD) was performed on samples to determine the crystallinity and molecular orientation in PCL fibres. The results revealed a gradual increase in crystallinity from 40% to 50% when fibre diameter was reduced from 900 to 200 nm. However, the authors concluded that WAXD results were insufficient to justify the observed correlation between mechanical properties and diameter of PCL fibres [123]. They suggested that examination of crystalline morphology and supramolecular structure could explain the increase of the Young's modulus.

In a similar study, Chew *et al.* utilized the tensile testing method to measure the Young's modulus of electrospun PCL (M_w = 60,000) fibres with diameters in the range of 200 - 300 nm [127]. The authors reported that E of the PCL nanofibres were at least twice as high as the modulus of the bulk material. However, they demonstrated that x-ray diffraction results did not show a significant difference in the crystalline fraction or perfection of the fibres compared with PCL films in order to explain the observed enhancement of mechanical properties [127].

Tan *et al.* also used a nano tensile tester (NanoBionix, MTS, USA) to characterize the tensile properties of PCL electrospun fibres [93]. The fibres were fabricated using 7.5 wt% PCL (M_n = 80,000) polymer solution with chloroform and methanol (3:1) as the solvent. They reported a tensile modulus of 120 ± 30 MPa for PCL fibres with diameters of 1.4 ± 0.3 μm [93] . The stress-strain curves obtained in their experiment demonstrated that mechanical properties such as the tensile strength and yield stress decreased as the fibre diameter was increased. However, they reported that they did not observe any apparent correlation between the Young's modulus and fibre diameter [93].

Due to the size difference (1.4 ± 0.3 μm vs. 100 - 400 nm) of PCL fibres that were examined in Tan *et al.*'s study and the difference in polymer solution concentration (7.5 wt% vs. 12 wt%) and the mechanical testing method (tensile testing vs. multipoint bending test), no direct comparison of the mechanical properties can be made between Tan *et al.*'s results and the Young's modulus that we found in our study. This is because the mechanical properties of polymers can vary with molecular weight, polymer concentration, and the processing technique. However, Tan *et al.*'s result is consistent with what we demonstrated in this study, showing that the Young's modulus is not size dependent, at least for d >100 nm.

Aristein *et al.* have discussed the abrupt increase in Young's modulus of polymer nanofibres by referring to the change in supramolecular microstructure [128]. The authors first performed elongation tests on single electrospun Nylon 6.6 nanofibres which yield an increasing trend in the Young's moduli of fibres with diameters < 500 nm. However, x-ray analysis revealed a mild, monotonous increase in crystallinity and orientation of the

crystalline domain in fibres with respect to change in diameter [128]. Also, the average size of the crystallites was found to be constant; approximately 4 nm for all fiber diameters. Therefore, the authors concluded that crystallinity could not explain the stiffening effect of nanofibres. Instead, they demonstrated that the supramolecular structures, consisting of aligned fragments of polymer chains, play a more dominant role in tensile deformation of nanofibres [128]. According to Aristein *et al.*, for each polymeric nanofibre, the Young's modulus may increase abruptly if the diameter is reduced beyond a critical value. For instance, the Young's modulus of polypyrole nanotube increases significantly for $d < 50$ nm [128, 122]. For PCL fibres examined in this study, further investigation is required for $d < 100$ nm to provide evidence of potential increase in the Young's modulus when the diameter is reduced beyond a critical value.

In summary, this study indicates conclusively that the Young's modulus of electrospun PCL ($M_n = 80,000$) nanofibres with diameters in the range of $100 - 400$ nm is similar to the modulus of the bulk material. The analytical model used in this study accounts for the effect of axial tensile forces due to stretching, and the residual tension in fibres. Comparison of this result with that of similar studies reported in the literature reveals that inaccurate assumptions could yield an overestimated Young's modulus, particularly when an AFM-based multi-point bending test is performed. On the other hand, tensile testing experiments performed on nanofibres require difficult manipulation and fibre alignment, and are therefore not as reliable as the AFM-based technique.

5.3 Young's Modulus of Collagen Fibres

5.3.1 Studies on As-spun Collagen Fibres

In a similar study conducted by Yang *et al.*, Young's moduli in the range of 1.4 − 7.5 GPa were obtained for as-spun electrospun collagen (type I from calf skin) fibres with diameters of 179 − 356 nm, using a multi-point bending test with an AFM [129]. Yang *et al.* also conducted another study on collagen fibrils from bovine Achilles tendon and obtained Young's moduli of 1.0 to 3.9 GPa for fibrils with diameters of 187 − 305 nm [130].

In another study, Joost A. J. van der Rijt *et al*. reported a Young's modulus of 2 − 7 GPa for single collagen type I fibrils from bovine Achilles tendon in the dry state [131]. The two ends of the fibril were attached to an AFM tip and a glass surface. As the fibril was pulled away from the glass with the tip of the cantilever, an optical microscope was used to monitor the stretching effect of the fibril to obtain the stress-strain curves from which the Young's moduli were obtained [131].

Wenger *et al*. also investigated the mechanical properties of collagen type I fibrils from rat tail using nanoindentation with AFM for fibrils with diameter of 50 to 200 nm [132]. The Young's modulus was found to be in the range of 5 to 11.5 GPa. The authors attributed this broad range to the natural variation in fibrils' properties, dehydration, and the accuracy of calibration [132].

In a recent study, Carlisle *et al*. investigated the stress-strain properties of single electrospun collagen type I nanofibres using three-point bending test with an atomic force microscope [133]. For fibres with diameters in the range of 302 ± 126 nm, a Young's modulus of 2.8 ± 0.4 GPa was obtained. They also reported that the Young's modulus increased as the fibre diameter was decreased [133]. However, it was not reported whether the effect of inherent tensile forces or the possible pre-existing strain in fibres were taken into account.

The Young's modulus of type I collagen fibres obtained in this study (1.66 − 13.9 GPa) is consistent with the reported values in the literature, and is significantly higher compared

with the modulus of PCL fibres. However, it should be noted that mechanical properties of hydrophilic polymers, such as collagen, strongly depend on their hydration state. In tissue engineering applications, scaffold materials are exposed to aqueous environment when implanted in the body, which can significantly influence their mechanical properties.

Joost A. J. van der Rijt et *al.* demonstrated that collagen fibres, in the wet state, i.e., in phosphate buffer saline (PBS), attains a much lower stiffness that is approximately 0.2 – 0.8 GPa [131]. Yang *et al.* also reported a range of 0.07 – 0.26 GPa for the Young's modulus of electrospun collagen (type I from calf skin) fibres after cross-linking with glutaraldehyde and immersion in PBS [129]. In another study, Yang *et al*. investigated the Young's modulus of collagen type I fibrils from bovine Achilles tendon in PBS buffer. For collagen fibrils which were cross-linked with 1-ethyl-3-(3-dimethylaminopropyl) carbodiimide hydrochloride (EDC) and N-hydroxysuccinimide (NHS), after being immersed in PBS, a Young's modulus of 0.06 to 0.14 GPa was obtained [130]. A similar result was obtained for native collagen fibrils examined in the same study [130]. These results indicate that the stiffness of collagen fibres decreases significantly, i.e., approximately by one order of magnitude, in aqueous environments.

The obtained Young's modulus for PCL nanofibres in this study is consistent with that of native single collagen fibres in their wet state. As PCL is highly hydrophobic, it is expected that its mechanical properties will not alter significantly after immersion in an aqueous environment. However, further investigation is necessary to confirm this hypothesis.

5.3.2 Genipin-Cross-Linked Collagen Fibres

Collagen fibres made by electrospinning are not stable in the wet state and disintegrate rapidly when immersed in an aqueous medium. Therefore, it is necessary to stabilize them using a cross-linking agent for cell culture applications. In this study genipin was used as a non-toxic cross-linking agent to stabilize the electrospun collagen nanofibres as previously established [89]. To our knowledge, this is the first time that the Young's modulus of genipin -cross-linked electrospun collagen type I fibres has been investigated.

In this study, the stiffness of genipin-cross-linked collagen fibres was found with a mean value of 21.95 GPa which is significantly higher than that of as-spun collagen fibres. In contrast, Yang *et al.*'s study on cross-linking of collagen type I fibrils with EDC and NH revealed no significant difference in the stiffness of fibres compared with their uncross-linked counterparts, both in PBS and in the dry state [130]. Also, in another study Yang *et al.* demonstrated that the Young's modulus of electrospun collagen type I fibres which were cross-linked with glutaraldehyde vapor was consistent with that of the uncross-linked fibres in the dry state [129]. In contrast, the Young's modulus decreased when the cross-linked fibres were immersed in PBS buffer [129]. However, it is difficult to make any direct comparison between the results obtained in this study and those reported by Yang *et al.*, due to the difference of collagen type and the cross-linking method used.

In summary, this study has demonstrated that genipin-cross-linked electrospun collagen fibres have a higher Young's modulus compared with their as-spun counterparts. However, it is possible to tune the stiffness and degradation of collagen fibres by controlling the cross-linking reaction conditions with genipin [89, 121]. Further investigation is required to determine whether the stiffness of genipin-cross-linked fibres decreases when immersed in PBS.

5.4 Biomedical Applications

In this study, the Young's modulus of PCL and collagen type I (as-spun and cross-linked) electrospun fibres was investigated in order to determine whether their stiffness is suitable for tissue engineering of the tympanic membrane. Although the majority of collagen fibres in the tympanic membrane are collagen type II [24], the information obtained from mechanical testing of as-spun and cross-linked collagen type I nanofibres can be used as a guide for future investigations on type II collagen nanofibres. This information is vital to control cell adhesion, migration and proliferation in tissue engineering applications, since cell behaviour and cell-scaffold interactions strongly depend on the stiffness of the substrate to which the cells anchor themselves. Table. 5.1 summarizes the results obtained from mechanical testing on PCL and collagen electrospun nanofibres.

Table. 5.1: Young's moduli of PCL, as-spun and cross-linked collagen nanofibres

Electrospun Fibre	Diameter	E (GPa)	Hydrophilicity	Degradation Rate
PCL (M_n : 80,000)	100 – 409 nm	0.48 ± 0.03	hydrophobic	slow
As-spun Type I Collagen	49 – 115 nm	1.66 – 13.9	hydrophilic	unstable in aqueous solution
Genipin- Cross-linked Collagen	73 – 113 nm	8.22 – 40.1	hydrophilic	controllable

As is evident from Table. 5.1, genipin-cross-linked collagen fibres have a higher modulus compared with as-spun fibres. However, it is expected that the stiffness will decrease approximately by one order of magnitude when the fibres are exposed to aqueous solutions such as PBS. This is anticipated based on the results reported by Yang *et al.* for the stiffness of electrospun collagen (type I from calf skin) fibres. In Yang *et al.*'s study, the Young's modulus of fibres was reduced to a range of 0.07 – 0.26 GPa after cross-linking with glutaraldehyde and immersion in PBS [129]. In another study conducted by the same group, Young's modulus in the range of 0.06 to 0.14 GPa was obtained for collagen fibres which were cross-linked with EDC-NHS and were immersed in PBS solution [130]. It should be noted that it is not possible to make a direct comparison between the results obtained in this study with those reported by Yang *et al.* due to the difference in collagen type and the cross-linking method used. However, it is possible that genipin- cross-linked collagen fibres attain a stiffness of ~ 2 GPa, similar to that of the natural collagen fibres, after immersion in PBS. In contrast, since PCL is hydrophobic, it does not absorb significant amounts of water in PBS; as a result, the stiffness of PCL fibres is not expected to decrease significantly.

In summary, both PCL and collagen are promising scaffold materials for tissue engineering applications. PCL is a synthetic biocompatible polyester with a slow rate of degradation. Moreover, due to its hydrophobicity, it is anticipated that the mechanical

properties of electrospun PCL nanofibres will not significantly change in cell culture medium. In contrast, electrospun collagen fibers require stabilization before immersion in aqueous environments. However, the advantage of collagen over PCL is that its rate of degradation is tunable by controlling the degree of cross-linking. As a result, both types of fibers are considered as promising scaffold materials, and will be investigated further for tissue engineering of the tympanic membrane.

Chapter 6: Conclusions and Future Work

6.1 Summary and Conclusions

In this study, the Young's moduli of individual electrospun poly(caprolactone) (PCL) fibres as well as as-spun and cross-linked collagen nanofibres were investigated using multi-point bending test with an atomic force microscope (AFM). Single nanofibres suspended over trenches in silicon substrates were subjected to bending test using an AFM cantilever with pre-determined spring constant. Force curves were obtained using the AFM's force volume mode and the slope of the contact region in each force curve was measured to determine the elastic moduli of single suspended nanofibres. The data obtained from the relative slopes of the force spectra were analyzed using four different beam models.

First, the Euler-Bernoulli beam theory was used based on the assumption that the fibres experienced "pure bending" and the internal shear stress and tensile forces had negligible effect on fibres' bending behaviour. However, the obtained results revealed an apparent dependence on diameter and aspect ratio. As a result, the Timoshenko beam model was applied to investigate whether the influence of shear stress was significant. However, this model was satisfactory only for large aspect ratios and predicted an unreasonably large Young's modulus. Finally, the models due to Heidelberg *et al*. and Hudson *et al.* were used to examine the effect of axial tensile forces induced as a result of stretching, and the effect of any initial tension due to the pre-existing strain in the fibres, respectively.

Using Hudson *et al.*'s model, consistent results with a mean value of 0.48 ± 0.03 GPa were obtained for the Young's modulus of electrospun PCL nanofibres with diameters in the range of $100 - 400$ nm. This result is consistent with the Young's modulus of bulk PCL. Analyzing the results using Heidelberg *et al*. and Hudson *et al.*'s models eliminated the apparent dependence on diameter and aspect ratio, indicating that inaccurate assumptions could yield an overestimated Young's modulus. Also, comparison of this result with those obtained from previous models and those of similar studies reported in

the literature reveals the importance of considering the tension due to elongation and the possibility of pre-existing strain in fibres.

Using Hudson *et al.*'s model, Young's moduli in the range of 1.66 – 13.9 GPa and 8.22 – 40.1 GPa were found for as-spun and genipin-cross-linked collagen fibres, respectively. The genipin-cross-linked electrospun collagen fibres have a higher Young's modulus compared with that of as-spun fibres; however, it is possible to tune the stiffness of collagen fibres by controlling the cross-linking conditions. Moreover, the Young's modulus of PCL electrospun fibres found in this study is close to that of single collagen fibres in their wet state, as reported in the literature. It is anticipated that the Young's modulus of PCL fibres will not significantly change in aqueous environments, since PCL is a hydrophobic polymer.

This study demonstrated that the stiffness of electrospun PCL and collagen fibres are promising for tissue engineering applications. Although the majority of collagen fibres in the tympanic membrane are collagen type II, the information obtained from this study on collagen type I can be used as a guide for future investigations on nanomechanical characterization of other types of collagen.

6.2 Future Work

The focus of this work was to investigate the potential application of poly(caprolactone) (PCL) and collagen nanofibrous scaffolds for tissue engineering of the tympanic membrane.

In this study, the Young's modulus of electrospun PCL and collagen type I (as-spun and genipin-cross-linked) fibres were determined in the dry state. Further investigation is required to determine whether the stiffness of PCL and genipin-cross-linked fibres decreases when immersed in cell culture media.

Further *in-vitro* studies can be carried out to test the impact of mechanical properties of electrospun PCL and collagen nanofibrous scaffolds on cell attachment, proliferation and migration. Furthermore, it is necessary to investigate the mechanical properties of collagen type II, as it is the most abundant collagen in the tympanic membrane.

The next stage would be to control the alignment of PCL and collagen nanofibres in the tissue engineering scaffolds in order to mimic the radial and circumferential orientation of collagen fibres in the tympanic membrane.

Future work would be also focused on investigating the nanomechanics of core-shell electrospun PCL and collagen nanofibres. The core-shell structure is essential to encapsulate and release bioactive molecules in a controlled fashion in order to promote cell attachment and proliferation.

References

[1]   P.J Govaerts *et al.*, "Histological study of the thin replacement membrane of human tympanic membrane perforations" *Acta Oto-Laryngologica,* vol. 105, pp. 297-302, 1988.

[2]   K. N. O'Connor *et al.*, "Tympanic Membrane Collagen Fibers: A Key to High-Frequency Sound Conduction" *The Laryngoscope,* vol. 118, no. 3, pp. 483-490, 2008.

[3]   A. Parekh *et al.*, "Repair of the Tympanic Membrane with Urinary Bladder Matrix" *The Laryngoscope,* vol. 119, pp. 1206-1213, 2009.

[4]   S. Saraç, and B. Gürsel *et al.*, "Use of Homograft Dehydrated Temporal Fascia in Tympanoplasty" *Otology & Neurotology,* vol. 23, pp. 416-421, 2002.

[5]   S. Yetiser, and Y. Hidir, "Temporalis Fascia and Cartilage-Perichondrium Composite Shield Grafts for Reconstruction of the Tympanic Membrane" *Annals of Otology, Rhinology & Laryngology,* vol. 118, no. 8, pp. 570-574, 2009.

[6]   F. Oktem *et al.*, "Vibration Characteristics of Grafts for the Tympanic Membrane" *Advances in Therapy,* vol. 24, no. 1, pp. 81-90, 2007.

[7]   A. Raj *et al.*, "Sutureless tympanoplasty using acellular dermis" *American Journal of Otolaryngology–Head and Neck Medicine and Surgery,* vol. 32, no. 2, pp. 96-99, 2011.

[8]   D. E. Discher, P. Janmey, Y. Wang, "Tissue Cells Feel and Respond to the Stiffness of Their Substrate" *Science,* vol. 310, no. 5751, pp. 1139-1143, 2005.

[9]   J. S. Choi *et al.*, "The influence of electrospun aligned poly(ε-caprolactone)/collagen nanofiber meshes on the formation of self-aligned skeletal muscle myotubes" *Biomaterials,* vol. 29, pp. 2899-2906, 2008.

[10] A. C. Albertsson and I. K. Varma *et al.*, "Recent developments in ring opening polymerization of lactones for biomedical applications" *Biomacromolecules,* vol. 4, no. 6, pp. 1466-1486, 2003.

[11] E. S. Place *et al.*, "Synthetic polymer scaffolds for tissue engineering" *Chemical Society Reviews,* vol. 38, pp. 1139-1151, 2009.

[12] G. H. Kim, "Electrospun PCL nanofibres with anisotropic mechanical properties as a biomedical scaffold" *Biomedical Materials,* vol. 3, no. 2, p. 025010 (8pp), 2008.

[13] I. U. Allan *et al.*, "The use of Confocal Laser Scanning Microscopy to Assess the Potential Suitability of 3D Scaffolds for Tissue Regeneration, by Monitoring Extra-Cellular Matrix

Deposition and by Quantifing Cellular Infiltration and Proliferation" *Soft Materials,* vol. 7, no. 4, pp. 319-341(23), 2009.

[14] S. A. Sell *et al.,* "Electrospinning of collagen/biopolymers for regenerative medicine and cardiovascular tissue engineering" *Advanced Drug Delivery Reviews,* vol. 61, p. 1007–1019, 2009.

[15] E. Zussman *et al.,* "Tensile deformation of electrospun nylon-6,6 nanofibers" *Journal of Polymer Science Part B: Polymer Physics,* vol. 44, no. 10, pp. 1482 - 1489, 2006.

[16] R. Agrawal *et al.,* "Elasticity Size Effects in ZnO Nanowires-A Combined Experimental-Computational Approach" *Nano Letters,* vol. 8, no. 11, pp. 3668-3674, 2008.

[17] E. P. S. Tan, C. T. Lim, "Novel approach to tensile testing of micro- and nanoscale fibers" *Review of Scientific Instruments,* vol. 75, no. 8, pp. 2581-2585, 2004.

[18] M. F. Yu *et al.,* "Tensile Loading of Ropes of Single Wall Carbon Nanotubes and their Mechanical Properties" *Physical Review Letters,* vol. 84, no. 24, p. 5552=5555, 2000.

[19] J. P. Salvetat *et al.,* "Elastic and Shear Moduli of Single-Walled Carbon Nanotube Ropes" *Physical Review Letters,* vol. 82, no. 5, pp. 945-947, 1999.

[20] O. A. Bauchau, and J. I. Craig, "Euler-Bernoulli Beam Theory" in *Structural Analysis: With Applications to Aerospace Structures*, Springer, 2009, pp. 173-221.

[21] G. Guhados , W. Wan , and J. L. Hutter , "Measurement of the Elastic Modulus of Single Bacterial Cellulose Fibers Using Atomic Force Microscopy" *Langmuir,* vol. 21, no. 14, p. 6642–6646, 2005.

[22] K. Stenfeldt, C. Johansson, and S. Hellstrom, "The collagen structure of the tympanic membrane" *Otolaryngol Head Neck Surgery,* vol. 132, pp. 293-298, 2006.

[23] R. Probst, G. Grevers, and H. Iro, "Tympanic Cavity" in *Basic Otorhinolaryngology: A Step-by-Step Learning Guide* , New York, Georg Thieme Verlag, 2006, pp. 228-229.

[24] J. Knutsson, D. Bagger-Sjö¨ba¨ck, and M. von Unge, "Collagen Type Distribution in the Healthy Human Tympanic Membrane" *Otology & Neurotology ,* vol. 30, pp. 1225-1229, 2009.

[25] W. J. Lee *et al.,* "Virtual biopsy of rat tympanic membrane using higher harmonic generation microscopy" *Journal of Biomedical Optics,* vol. 15, no. 4, p. 046012 (5), 2010.

[26] S. Puria, and C. Steele, "Tympanic-membrane and malleus–incus-complex co-adaptations for high-frequency hearing in mammals" *Hearing Research,* vol. 263, pp. 183-190, 2010.

[27] I. Kawabata, and H. F. Ishii., "Fibre arrangement in the tympanic membrane" *Acta Otolaryng* , vol. 72, pp. 243-256, 1971.

[28] A. P. Johnson, L. A. Smallman, S. E. Kent, " The mechanism of healing of tympanic membrane perforations" *Acta Otolaryngol,* vol. 109, p. 406–415, 1990.

[29] T. Zahnert *et al.*, "Experimental Investigations of the Use of Cartilage in Tympanic Membrane Reconstruction" *The American Journal of Otology,* vol. 21, p. 322–328 , 2000.

[30] J. D. Vos *et al.*, " Use of AlloDerm in Type I Tympanoplasty: A comparison with Native Tissue Grafts" *The American Laryngological,* vol. 115, no. 9, pp. 1599-602, 2005.

[31] J. F. Cooley, "Apparatus for electrically dispersing fluids". US Patent 692631, 1902.

[32] W. J. Morton, "Method of dispersing fluids". US Patent 705691, 1902.

[33] A. Formhals, "Process and apparatus for preparing artificial threads". US Patent 1 ,975, 504, 1934.

[34] W. E. Teo, and S. Ramakrishna, "A review on electrospinning design and nanofibre assemblies" *Nanotechnology,* vol. 17, p. R89–R106, 2006.

[35] Z. M. Huanga *et al.*, "A review on polymer nanofibers by electrospinning and their applications in nanocomposites" *Composites Science and Technology,* vol. 63, p. 2223–2253, 2003.

[36] I. S. Chronakis, "Novel nanocomposites and nanoceramics based on polymer nanofibers using electrospinning process—A review" *Journal of Materials Processing Technology,* vol. 167, p. 283–293, 2005.

[37] S. G. Kumbar *et al.*, "Electrospun nanofiber scaffolds: engineering soft tissues" *Biomedical Materials,* vol. 3, p. 034002 (15pp), 2008.

[38] Y. M. Shin *et al.*, "Electrospinning: A whipping fluid jet generates submicron polymer fibers," *Applied Physics Letters,* vol. 78, no. 8, pp. 1-3, 2001.

[39] S. V. Fridrikh *et al.*, "Controlling the Fiber Diameter during Electrospinning" *Physical Review Letters,* vol. 90, no. 14, pp. 144502(1-4), 2003.

[40] S. V. Fridrikh *et al.*,"Controlling the fiber diameter during electrospinning" *Phys Rev Lett,* vol. 90, p. 144502, 2003.

[41] T. A. Kowelewski, S. Bło´nski, and S. Barral, "Experiments and modelling of electrospinning process" *Bull. Pol. Ac.: Tech.,* vol. 53, no. 4, pp. 385-394, 2005.

[42] S. A. Theron, E. Zussman, and A. L. Yarin , "Experimental investigation of the governing parameters in the electrospinning of polymer solutions" *Polymer,* vol. 45, p. 2017–30, 2004.

[43] M. A. Costolo *et al.*, " A nonlinear system model for electrospinning sub-100 nm polyacrylonitrile fibres" *Nanotechnology ,* vol. 19, p. 035707 (9pp), 2008.

[44] Q. P. Pham, U. Sharma, and A. G. Mikos "Electrospinning of Polymeric Nanofibers for Tissue Engineering Applications: A Review" *Tissue Engineering,* vol. 12, no. 5, pp. 1197-1211, 2006.

[45] X. H. Zong *et al*., "Structure and process relationship of electrospun bioabsorbable nanofiber membranes" *Polymer,* vol. 43, no. 4403, 2002.

[46] C. X. Zhang *et al*., "Study on morphology of electrospun poly(vinyl alcohol) mats" *Eur. Polym.,* vol. 41, no. 423, 2005.

[47] W. Zuo *et al*., "Experimental study on relationship between jet instability and formation of beaded fibers during electrospinning" *Polym. Eng. Sci.,* vol. 45, no. 704, 2005.

[48] L. Wannatong, A. Sirivat, and P. Supaphol, "Effects of solvents on electrospun polymeric fibers: preliminary study on polystyrene" *Polym. Int.,* vol. 53, no. 1851, 2004.

[49] X. Y. Yuan *et al*., "Morphology of ultrafine polysulfone fibers prepared by electrospinning" *Polym. Int,* vol. 53, no. 1704, 2004.

[50] J. M. Deitzel *et al*., "The effect of processing variables on the morphology of electrospun nanofibers and textiles" *Polymer,* vol. 42, no. 261, 2001.

[51] C. S. Ki *et al*., "Characterization of gelatin nanofiber prepared from gelatin-formic acid solution" *Polymer,* vol. 46, no. 5094, 2005.

[52] X. Y. Geng, O. H. Kwon, and J. H. Jang, "Electrospinning of chitosan dissolved in concentrated acetic acid solution" *Biomaterials,* vol. 26, no. 5427, 2005.

[53] C. J. Buchko *et al*., "Processing and microstructural characterization of porous biocompatible protein polymer thin films" *Polymer,* vol. 40, no. 7397, 1999..

[54] J. S. Lee *et al*., "Role of molecular weight of atactic poly(vinyl alcohol) (PVA) in the structure and properties of PVA nanofabric prepared by electrospinning" *J. Appl. Polym. Sci.,* vol. 93, no. 1638, 2004.

[55] L. Huang *et al*., "Engineered collagen-PEO nanofibers and fabrics" *J.Biomater. Sci. Polym. Ed.,* vol. 12, no. 979, 2001.

[56] P. Gupta *et al*., "Electrospinning of linear homopolymers of poly(methylmethacrylate): exploring relationships between fiber formation, viscosity, molecular weight and concentration in a good solvent" *Polymer,* vol. 46, no. 4799, 2005.

[57] T. Jarusuwannapoom *et al*., "Effect of solvents on electro-spinnability of polystyrene solutions and morphological appearance of resulting electrospun polystyrene fibres" *Eur. Polym.,* vol. 41, no. 409, 2005.

[58] Z. Jun *et al*., "Poly-L-lactide nanofibers by electrospinning–influence of solution viscosity and electrical conductivity on fiber diameter and fiber morphology" *E-Polymers,* 2003.

[59] M. M. Demir *et al*., "Electrospinning of polyurethane fibers" *Polymer,* vol. 43, no. 3303, 2002.

[60] B. Duan *et al*., "Electrospinning of chitosan solutions in acetic acid with poly(ethylene oxide)" *J. Biomater. Sci. Polym. Ed.,* vol. 15, no. 797, 2004.

[61] M. G. Mckee *et al*., "Correlations of solution rheology with electrospun fiber formation of linear and branched polyesters" *Macromolecule,* vol. 37, no. 1760, 2004.

[62] H. Chen, and Y. L. Hsieh, "Ultrafine hydrogel fibers with dual temperature- and pH-responsive swelling behaviors" *J. Polym. Sci. A. Polym. Chem.,* vol. 42, no. 6331, 2004.

[63] C. Mit-Uppatham, M. Nithitanakul, and P. Supaphol, "Ultrafine electrospun polyamide-6 fibers: effect of solution conditions on morphology and average fiber diameter" *Macromol. Chem. Phys.,* vol. 205, no. 2327, 2004.

[64] H. Fong, I. Chun, and D. H. Reneker, "Beaded nanofibers formed during electrospinning" *Polymer ,* vol. 40, no. 4585, 1999.

[65] C. L. Casper *et al*., "Controlling surface morphology of electrospun polystyrene fibers: effect of humidity and molecumolecular weight in the electrospinning process" *Macromolecules,* vol. 37, no. 573, 2004.

[66] A. L. Szentivanyi *et al*., "A review of developments in electrospinning technology: New opportunities for the design of artificial tissue structures" *Int J Artif Organs,* vol. 34, no. 10, pp. 986-997, 2011.

[67] D. Zhang and J. Chang, "Electrospinning of Three-Dimensional Nanofibrous Tubes with Controllable Architectures," *Nano Letters,* vol. 8, no. 10, pp. 3283-3287, 2008.

[68] M. J. Dalby *et al*., "The control of human mesenchymal cell differentiation using nanoscale symmetry and disorder" *Nature Materials,* vol. 6, pp. 997-1003, 2007.

[69] D. Li, Y. Wang, and Y. Xia , "Electrospinning Nanofibres as Uniaxially Aligned Arrays

and Layer-by-Layer Stacked Films" *Advanced Materials,* vol. 16, no. 4, pp. 361-366, 2004.

[70]   Kenneth Kar Ho Wong, "Cell Compatible Electrospun Poly(vinyl alcohol) Fibers for Tissue Regeneration," Thesis, 2010.

[71]   C.Y. Xu , R. Inai, M. Kotaki, S. Ramakrishna, "Aligned biodegradable nanofibrous structure: a potential scaffold for blood vessel engineering" *Biomaterials,* vol. 25, p. 877–886, 2004.

[72]   X. Wang *et al.,* "Continuous polymer nanofiber yarns prepared by self-bundling electrospinning method" *Polymer,* vol. 49, p. 2755–2761, 2008.

[73]   H. Pan *et al.,* "Continuous aligned polymer fibers produced" *Polymer,* vol. 47, p. 4901–4904, 2006.

[74]   H. Jiang *et al.,* "A facile technique to prepare biodegradable coaxial electrospun nanofibers for controlled release of bioactive agents" *Journal of Controlled Release,* vol. 108, no. 2-3, pp. 237-243, 2005.

[75]   Y. Yang *et al.,* "Release pattern and structural integrity of lysozyme encapsulated in core-sheath structured poly(dl-lactide) ultrafine fibers prepared by emulsion electrospinning" *European Journal of Pharmaceutics and Biopharmaceutics,* vol. 69, no. 1, pp. 106-116, 2008.

[76]   R. A. Thakur *et al.,* "Electrospun nanofibrous polymeric scaffold with targeted drug release profiles for potential application as wound dressing" *International Journal of Pharmaceutics,* vol. 364, no. 1, pp. 87-93, 2008.

[77]   Y. Z. Zhang *et al.,* "Coaxial electrospinning of (fluorescein isothiocyanate-conjugated bovine serum albumin)-encapsulated poly(epsilon-caprolactone) nanofibers for sustained release" *Biomacromolecules,* vol. 7, no. 4, pp. 1049-57, 2006.

[78]   Y. Zhang *et al.,* "Electrospinning of gelatin fibers and gelatin/PCL composite fibrous scaffolds" *Biomed Mater Res B Appl Biomater,* vol. 72, no. 1, pp. 156-65, 2005.

[79]   H. Jiang *et al.,* "A facile technique to prepare biodegradable coaxial electrospun nanofibers for controlled release of bioactive agents" *J Control Release,* vol. 108, no. 2-3, pp. 237-43, 2005.

[80]   A. Saraf *et al.,* "Fabrication of Nonwoven Coaxial Fiber Meshes by Electrospinning" *Tissue Eng Part C Methods,* 2009.

[81]   P. Fratzl, "Collagen Diversity, Synthesis, and Assembly" in *Collagen: Structure and Mechanics*, Germany, Springer, 2008, pp. 15-22.

[82] N. T. Wright, and J. D. Humphrey, "Denaturation of Collagen Via Heating : An Irreversible Rate Process" *Annu. Rev. Biomed. Eng,* vol. 4, pp. 109-28, 2002.

[83] M. J. Buehler, "Nature designs tough collagen: Explaining the nanostructure of collagen fibrils" *Applied Physical Sciences,* vol. 103, no. 33, p. 12285–12290, 2006.

[84] A. Jayakrishnan, and S. R.Jameela, "Glutaraldehyde as a fixative in bioprosthesis and drug delivery matrices" *Biomaterials,* vol. 17, pp. 471-484, 1996.

[85] J. H. Bowers, and C. W. Cater, "Crosslinking of collagen" *J Appl Chem ,* vol. 14, pp. 296-304, 1964.

[86] J. H. Bowers, and C. W. Cater , "The reaction of glutaraldehyde with proteins and other biological materials" *JMicrosc Soc ,* vol. 85, pp. 193-200, 1966.

[87] J. M. McPherson, S. Sawamura, and R. Armstrong, "An examination of the biologic response to injectable, glutaraldehyde cross-linked collagen" *J Biomed Mater,* vol. 20, pp. 93-107, 1986.

[88] C. P. Barnes *et al*.,"Cross-linking electrospun type II collagen tissue engineering scaffolds with carbodiimide in ethanol" *Tissue Engineering,* vol. 13, no. 7, pp. 1593-605, 2007.

[89] M. Mekhail *et al*., "Genipin-Cross-linked Electrospun Collagen Fibers" *Journal of Biomaterials Science,* vol. 0, pp. 1-19, 2010.

[90] J. S. Choi *et al*., "The influence of electrospun aligned polycaprolactone)/collagen nanofiber meshes on the formation of self-aligned skeletal muscle myotubes" *Biomaterials,* vol. 29, no. 19, pp. 2899-906, 2008.

[91] S. Eshraghi, and S. Das, "Mechanical and microstructural properties of polycaprolactone scaffolds with one-dimensional, two-dimensional, and three-dimensional orthogonally oriented porous architectures produced by selective laser sintering" *Acta Biomater,* vol. 6, no. 7, pp. 2467-76, 2010.

[92] G. H. Kim, "Electrospun PCL nanofibers with anisotropic mechanical properties as a biomedical scaffold" *Biomedical Materials,* vol. 3, no. 2, p. 025010 (8), 2008.

[93] E. P. S. Tan, S. Y. Ng, and C. T. Lim, "Tensile testing of a single ultrafine polymeric fiber" *Biomaterials,* vol. 26, p. 1453–1456, 2005.

[94] S. Chan *et al*., "Tensile Stress-Strain Response of Small-diameter Electrospun Fibers" Agilent Technologies, 2012.

[95] E. P. S. Tan, and C. T. Lim, "Mechanical characterization of nanofibers – A review" *Composites Science and Technology,* vol. 66, p. 1102–1111, 2006.

[96] W. Ding *et al.*, "Mechanics of crystalline boron nanowires" *Composites Science and Technology,* vol. 66, p. 1112–1124, 2006.

[97] S. Baker *et al.*, "The mechanical properties of dry, electrospun fibrinogen fibers" *Materials Science and Engineering C,* vol. 32, pp. 215-221, 2012.

[98] K.Y. Hwang *et al.*, "Mechanical characterization of nanofibers using a nanomanipulator and atomic force microscope cantilever in a scanning electron microscope" *Polymer Testing,* vol. 29, p. 375–380, 2010.

[99] X. Li *et al.*, "Nanoindentation of silver Nanowires" *Nanoletters,* vol. 3, no. 11, p. 1495–8, 2003.

[100] C. A. Clifford *et al.*, "Nanomechanicalmeasurementsofhairasanexampleofmicro-fibreanalysis using atomicforcemicroscopynanoindentation" *Ultramicroscopy,* vol. 114, pp. 38-45, 2012.

[101] J. Domke, and M. Radmacher "Measuring the elastic properties of thin polymer films with the atomic force microscope" *Langmuir,* vol. 14, no. 12, p. 3320–5, 1998.

[102] D. A. Dikin *et al.*, "Resonance vibration of amorphous SiO2 nanowires driven by mechanical or electrical field excitation" *Applied Physics,* vol. 93, no. 1, pp. 226-30, 2003.

[103] P. Poncharal *et al.*, "Electrostatic deflections and electromechanical resonances of carbon nanotubes" *Science,* vol. 283, no. 5407, p. 1513–6., 1999.

[104] Z. L. Wang, P. Poncharal, W. A. de Heer, "Nanomeasurements of individual carbon nanotubes by in situ TEM" *Pure Appl Chem,* vol. 72, no. 1-2, pp. 209-19, 2000.

[105] X. D. Bai *et al.*, "Dual-mode mechanical resonance of individual ZnO nanobelts" *Applied Physics Letters,* vol. 82, no. 26, p. 4806–8, 2003.

[106] Q. Cheng and S. Wang, "A method for testing the elastic modulus of single cellulose fibrils via atomic force microscopy" *Composites: Part A,* vol. 39, p. 1838–1843, 2008.

[107] L. M. Bellan, J. Kameoka and H. G Craighead, "Measurement of the Young's moduli of individual polyethylene oxide and glass nanofibres" *Nanotechnology,* vol. 16, p. 1095–1099, 2005.

[108] A. J. M. Ferreira, "Chapter 10: Analysis of Timoshenko Beams" in *MATLAB Codes for Finite Element Analysis: Solids and Structures*, Springer, 2009, pp. 123-124.

[109] A. Heidelberg *et al.*, "A Generalized Description of the Elastic Properties of Nanowires" *Nano Letters,* vol. 6, no. 6, pp. 1101-1106, 2006.

[110] Y. Ikada, "Functions of Scaffold" in *Tissue Engineering: Fundamentals And Applications*, UK, Elsevier, 2006, pp. 1-3.

[111] S. Li, N. L'Heureux, and J. Elisseeff , "Cell Source" in *Stem cell and tissue engineering* , 5 Toh Tuck Link Singapore 596224, world scientific publishing Co. Pte. Ltd, 2011, pp. 3-8.

[112] J. Raghunath *et al*., "Biomaterials and scaffold design: key to tissue-engineering cartilage (Review article)" *Biotechnology and Applied Biochemistry ,* vol. 46, p. 73–84, 2007.

[113] R. Portner & C. Giese in *An Overview on Bioreactor Design, Prototyping and Process Control for Reproducible Three-Dimensional Tissue Culture, in Bioreactor Systems for Tissue Engineering*, Heidelberg , Germany, Springer-Verlag Berlin, 2009.

[114] A. Ratcliffe & L. E. Niklason "Bioreactors and bioprocessing for tissue engineering" *Ann. N. Y. Acad. Sci.,* vol. 961, p. 210–215, 2002.

[115] E. M. Lee, "Core-Shell Nanofibres for Heart Valve Leaflet Tissue Engineering," Master's Thesis (The University of Western Ontario), London, Ontario, Canada., 2011.

[116] J. Haley, " Bioactive scaffolds for tissue engineering" Master's Thesis (The University of Western Ontario), London, Ontario, Canada., 2009.

[117] 1996-99 Digital Instruments Veeco Metrology Group, "MultiMode™ SPM Instruction Manual Version 4.31ce".

[118] Timoshenko and J. M. Gere, Mechanics of Materials, 4th ed., Boston, MA: PWS, 1997.

[119] G. Guhados *et al*., "Simultaneous measurement of Young's and shear moduli of multiwalled carbon nanotubes using atomic force microscopy" *Journal of Applied Physics,* vol. 101, p. 033514, 2007.

[120] S. D. Hudson *et al*.,"Measurement of the Elastic Modulus of Spider Mite Silk Fibers Using Atomic Force Microscopy" *Journal of Applied Physics (submitted),* 2012.

[121] L. Bi *et al*., "Effects of different cross-linking conditions on the properties of genipin-cross-linked chitosan/collagen scaffolds for cartilage tissue engineering" *J Mater Sci: Mater Med,* vol. 22, p. 51–62, 2011.

[122] S. Cuenot, S. Demoustier-Champagne & B. Nysten, "Elastic modulus of polypyrrole nanotubes" *Phys. Rev. Lett.,* vol. 85, p. 1690–1693, 2000.

[123] S. Wong , A. Baji , & S. Leng, "Effect of fiber diameter on tensile properties of electrospun poly(3-caprolactone)" *Polymer,* vol. 49, p. 4713–4722, 2008.

[124] F. Croisier *et al*.,"Mechanical testing of electrospun PCL fibers," *Acta Biomaterialia,*

2011.

[125] B. Wen, J. E. Sader, J. J. Boland, "Mechanical properties of ZnO nanowires" *Phys. Rev. Lett,* vol. 101, p. 175502:1–4, 2008.

[126] S. H. Lee *et al*.,"Mechanical properties and creep behavior of lyocell fibers by nanoindentation and nano-tensile testing" *Holzforschung,* vol. 61, p. 254–260, 2007.

[127] S. Y. Chew *et al*., "Mechanical properties of single electrospun drug-encapsulated nanofibres" *Nanotechnology,* vol. 17, p. 3880–3891, 2006.

[128] A. Arinstein *et al*., "Effect of supramolecular structure on polymer nanofibre elasticity" *nature nanotechnology,* vol. 2, pp. 59-62, 2007.

[129] L. Yang *et al*., "Mechanical properties of single electrospun collagen type I fibers" *Biomaterials,* vol. 29, p. 955–962, 2008.

[130] L. Yang *et al*.,"Mechanical Properties of Native and Cross-linked Type I Collagen Fibrils" *Biophysical Journal,* vol. 94, p. 2204–2211, 2008.

[131] Joost A. J. van der Rijt *et al*.,"Micromechanical Testing of Individual Collagen Fibrils" *Macromol. Biosci,* vol. 6, p. 697–702, 2006.

[132] Marco P. E. Wenger, Laurent Bozec, Michael A. Horton, and Patrick Mesquida, "Mechanical Properties of Collagen Fibrils," *Biophysical Journal,* vol. 93, pp. 1255-1263, 2007.

[133] C.R. Carlisle, C. Coulais, and M. Guthold, "The mechanical stress–strain properties of single electrospun collagen type I nanofibers" *Acta Biomaterialia,* vol. 6, p. 2997–3003, 2010.

[134] L. D. Landau, and E. M. Lifshitz, *Theory of Elasticity*, 2nd Ed.; Pergamon Press, 1970

Appendix A –Models of Heidelberg et al. & Hudson et al.

In pure bending:

$$EI \, \frac{d^3 \delta(x)}{d \, x^3} = - \, \frac{F_{center}}{2} \qquad (A.1)$$

where $\delta(x)$ is the equilibrium displacement of fibre, F_{center} is the force applied at the centre of the fibre, E is the Young's modulus, and I is the area moment of inertia [120,134]. According to the clamped boundary conditions, the solution must satisfy:

1) $\delta(0) = 0$
2) $\delta'(0) = \delta'\left(\frac{L_0}{2}\right) = 0$

where L_0 is the length of the suspended portion of the fibre. The solution for F_{center} is determined as [134]:

$$F_{center} = \frac{192EI}{L_0{}^3} \, \delta_{center} \quad (A.2)$$

where δ_{center} is the deflection of the fibre at its centre. In small deflections, the vertical component of tension at position x is $\frac{Td\delta(x)}{dx}$; hence equation (A.1) can be rewritten as [134]:

$$EI \, \frac{d^3 \delta(x)}{d \, x^3} = - \, \frac{F_{center}}{2} + T \frac{d \, \delta(x)}{d \, x} \quad (A.3)$$

Heidelberg *et al.*'s solution of equation (A.3) using the clamped boundary conditions is [109]:

$$F_{center} = \frac{192EI}{L_0{}^3} \, f(\alpha)\delta_{center} \qquad (A.4)$$

where
$$f(\alpha) = \frac{\alpha}{48 - \frac{192 \tanh\left(\frac{\sqrt{\alpha}}{4}\right)}{\sqrt{\alpha}}} \qquad (A.5)$$

where α is a dimensionless parameter:
$$\alpha = \frac{TL_0^2}{EI} \qquad (A.6)$$

The tension due to stretching is $T = T_s$ given by [134]:

$$T_s = EA \frac{L-L_0}{L_0} = \frac{EA}{L_0} \int_0^{\frac{L_0}{2}} \left(\frac{d\delta}{dx}\right)^2 dx \qquad (A.7)$$

which yields the relationship between α and δ_{center} [109]:

$$\frac{\alpha \cosh^2\left(\frac{\sqrt{\alpha}}{4}\right)}{2 + \cosh\left(\frac{\sqrt{\alpha}}{2}\right) - 6\frac{\sinh\left(\frac{\sqrt{\alpha}}{2}\right)}{\sqrt{\alpha}}} \left(1 - 4\frac{\tanh\left(\frac{\sqrt{\alpha}}{4}\right)}{\sqrt{\alpha}}\right)^2 = \frac{A}{I} \delta_{center}^2 \qquad (A.8)$$

where A is the cross-sectional area of the fibre .

Hudson *et al.* extended the model of Heidelberg *et al.* to take into account the effect of initial tension T_0 ,such that $T = T_0 + T_s$. Hudson *et al.* determined the displacement of a fibre between $x = 0$ and $x = L_0/2$ subjected to an applied force F_{center} at the centre of the suspended length L_0 [120]:

$$\delta(x) = \frac{F_{center}}{2T} \left[x - \frac{L_0}{\sqrt{\alpha}} \frac{Sinh\left[\sqrt{\alpha}\left(\frac{x}{L_0} - \frac{1}{4}\right)\right] + Sinh\left(\frac{\sqrt{\alpha}}{4}\right)}{Cosh\left(\frac{\sqrt{\alpha}}{4}\right)}\right] \qquad (A.9)$$

The tension due to stretching, relative to the relaxed equilibrium length L_{eq} is:

$$T_s = EA \, \frac{L - L_0}{L_{eq}} = \frac{EA}{L_{eq}} \int_0^{L_0/2} \left(\frac{d\delta}{dx}\right)^2 dx \quad \text{(A.10)}$$

Substitution of equation (A.9) into equation (A.10) yields [120]:

$$\frac{T_s}{T} \frac{L_{eq}}{L_0} \left[\frac{\alpha \, Cosh^2(\frac{\sqrt{\alpha}}{4})}{2 + Cosh\left(\frac{\sqrt{\alpha}}{2}\right) - 6 \frac{Sinh\left(\frac{\sqrt{\alpha}}{2}\right)}{\sqrt{\alpha}}} \left(1 - 4 \frac{tanh(\frac{\sqrt{\alpha}}{4})}{\sqrt{\alpha}}\right)^2 \right] = \frac{A}{I} \delta^2_{centre} \quad \text{(A.11)}$$

Initial tension is defined as:

$$T_0 = EA \frac{L_0 - L_{eq}}{L_{eq}} \quad \text{(A.12)}$$

Therefore, equilibrium length is:

$$L_{eq} = L_0 \left(\frac{EA}{T_0 + EA}\right) \quad \text{(A.13)}$$

Using equation (A.13) and $T = T_0 + T_s$, equation (A.11) can be written as [120]:

$$\left(1 - \frac{T_0}{T}\right)\left(\frac{EA}{T_0 + EA}\right) \left[\frac{\alpha \, Cosh^2(\frac{\sqrt{\alpha}}{4})}{2 + Cosh\left(\frac{\sqrt{\alpha}}{2}\right) - 6 \frac{Sinh\left(\frac{\sqrt{\alpha}}{2}\right)}{\sqrt{\alpha}}} \left(1 - 4 \frac{tanh(\frac{\sqrt{\alpha}}{4})}{\sqrt{\alpha}}\right)^2 \right] = \frac{A}{I} \delta^2_{centre}$$

$$\text{(A.14)}$$

Appendix B – TEM Images of Solid & Core-Shell PCL Fibres


```
May25-PCL-PEG9.tif
Print Mag: 11000x @ 51 mm          500 nm
14:05 05/25/12                     HV=100kV
TEM Mode: Imaging                  Direct Mag: 19000x
                                   X: 689.464 Y: 179.637
                                   Biotron UWO
```



```
May24-PCL-PEG6.tif
Print Mag: 14500x @ 51 mm          500 nm
13:59 05/24/12                     HV=80kV
TEM Mode: Imaging                  Direct Mag: 25000x
Microscopist: JC                   X: 161.118 Y: -526.275
                                   Biotron UWO
```

May24-PCL-PEG5.tif
Print Mag: 7830x @ 51 mm
13:45 05/24/12
TEM Mode: Imaging
Microscopist: JC

500 nm
HV=80kV
Direct Mag: 13500x
X:-36.353 Y: -21.01
Biotron UWO
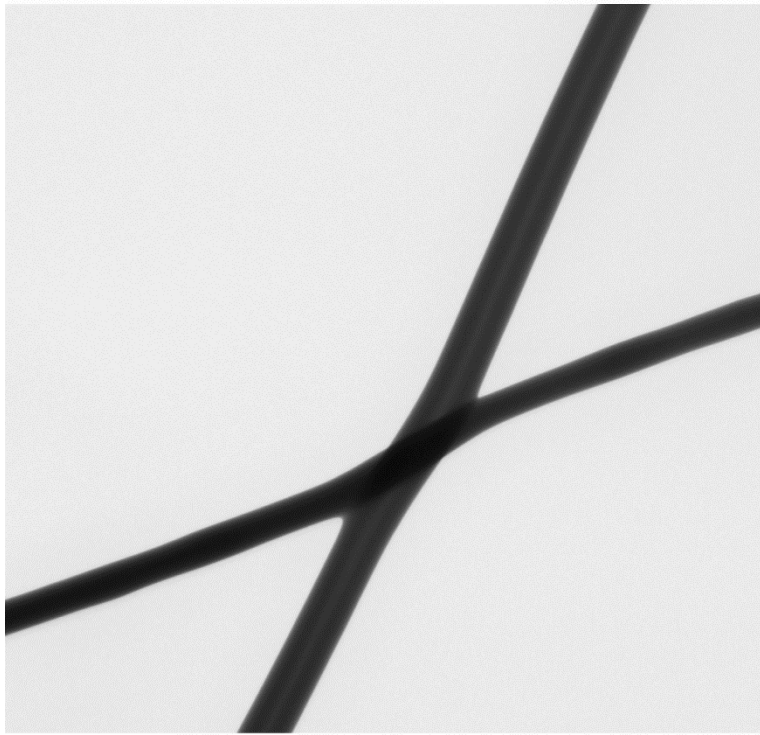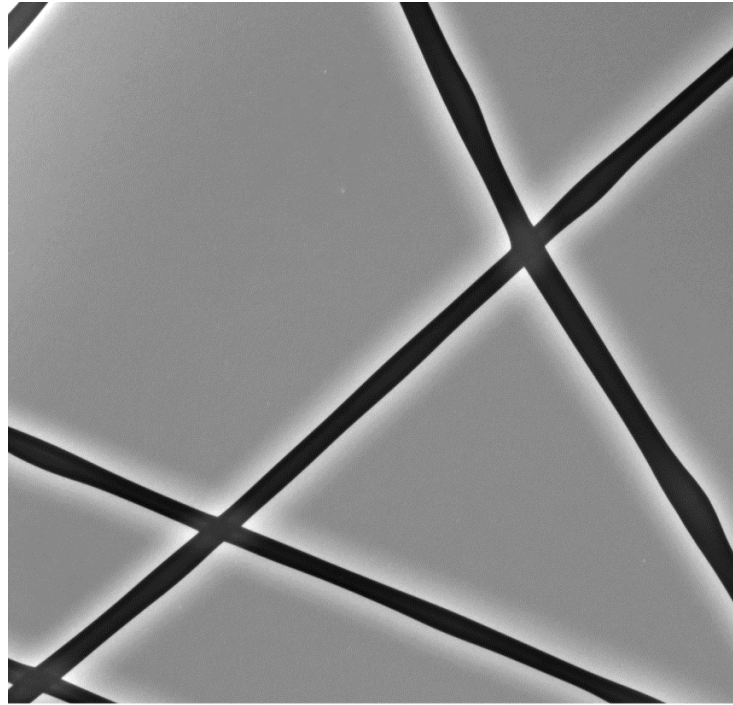

May24-PCL-PEG4.tif
Print Mag: 7830x @ 51 mm
13:39 05/24/12
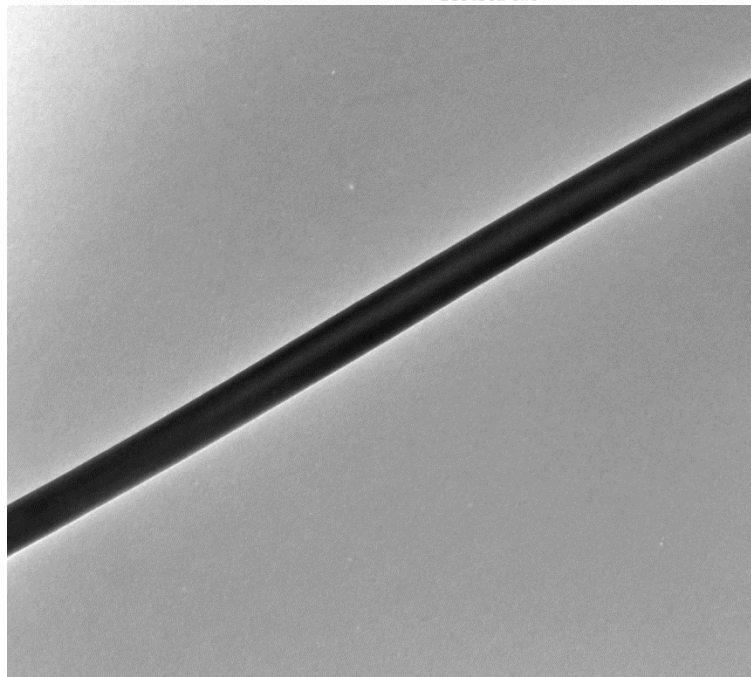TEM Mode: Imaging
Microscopist: JC

500 nm
HV=80kV
Direct Mag: 13500x
X:-93.05 Y: -127.84
Biotron UWO

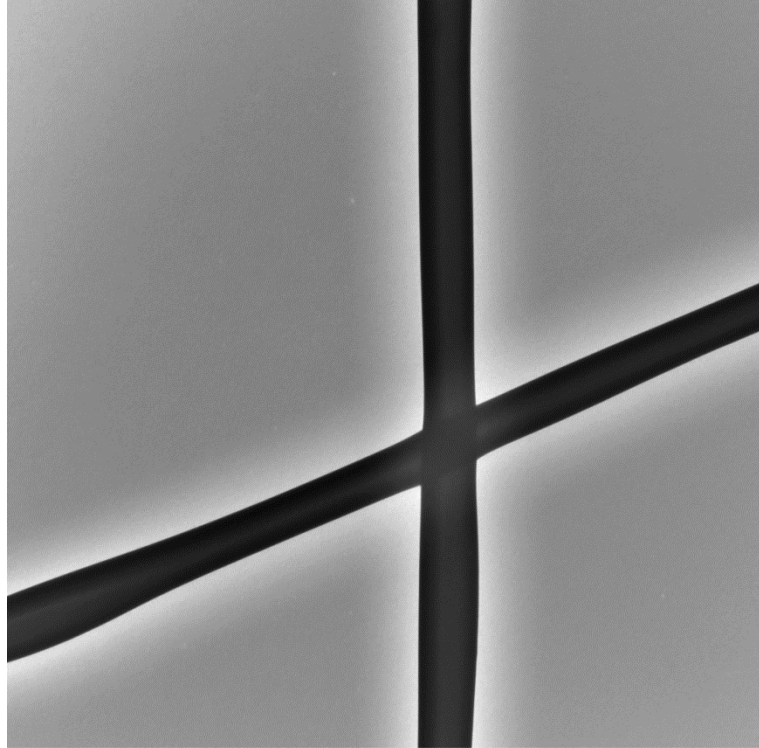# *Appendix C- TEM Images of Solid & Core-Shell Collagen Fibres*

collagen PEG 36.tif
Print Mag: 841x @ 51 mm
17:00 07/18/12
TEM Mode: Imaging

10 microns
HV=80kV
Direct Mag: 1450x
X: 251.143 Y: -304.261
Biotron UWO

collagen PEG 5.tif
Print Mag: 6070x @ 51 mm
16:13 07/18/12
TEM Mode: Imaging

500 nm
HV=80kV
Direct Mag: 10500x
X:-.046 Y: -804.022
Biotron UWO

collagen PEG 37.tif
Print Mag: 1970x @ 51 mm
17:01 07/18/12
TEM Mode: Imaging

2 microns
HV=80kV
Direct Mag: 3400x
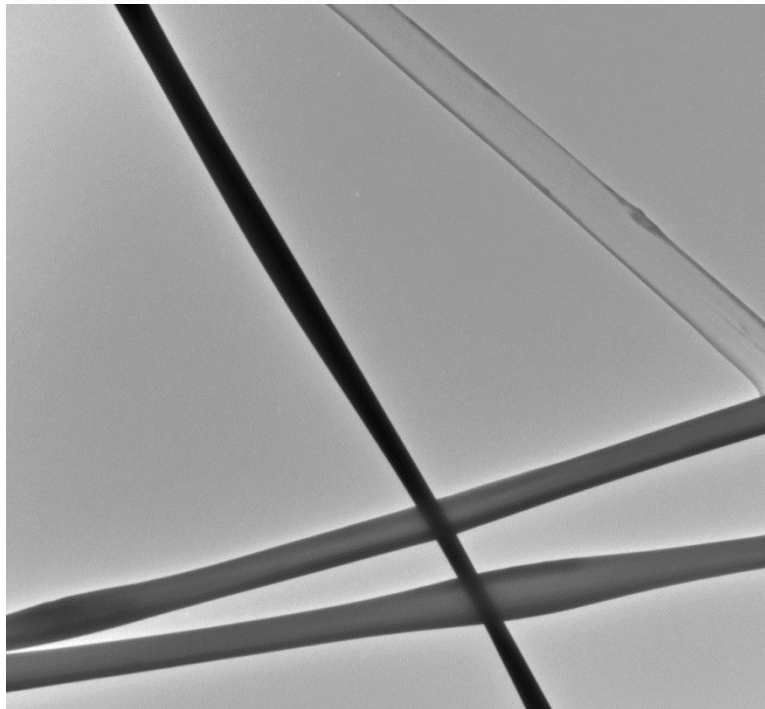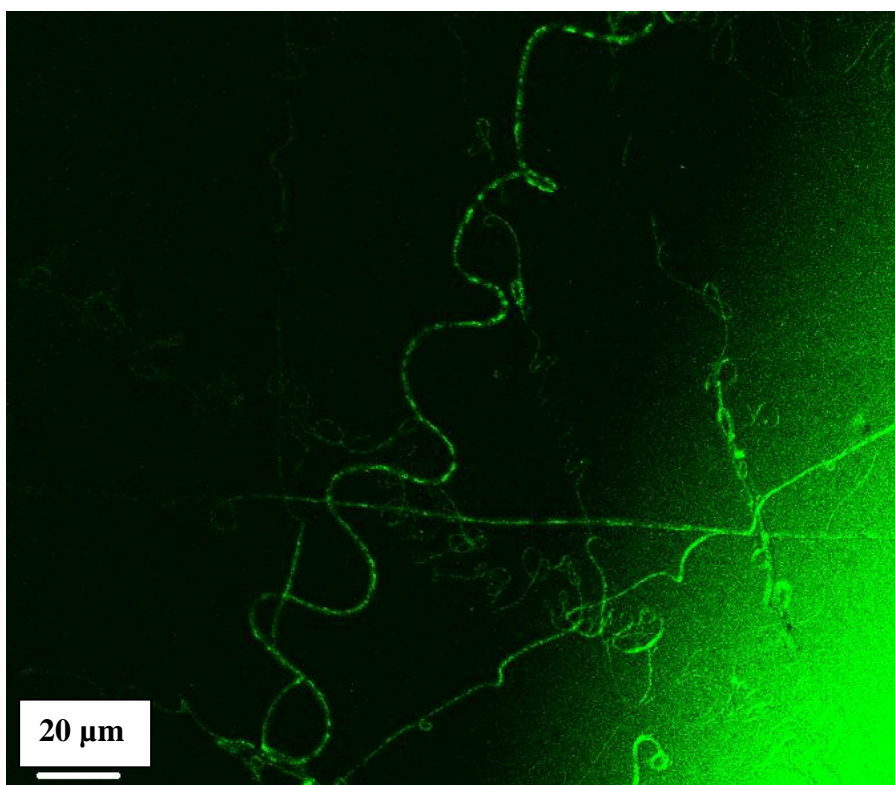X: 249.702 Y: −316.309
Biotron UWO

collagen PEG 18.tif
Print Mag: 1970x @ 51 mm
16:37 07/18/12
TEM Mode: Imaging

2 microns
HV=80kV
Direct Mag: 3400x
X:−462.067 Y:−535.886
Biotron UWO

Appendix D – Confocal Image of Core-Shell PCL Fibres

20 μm

Curriculum Vitae
Sara Makaremi M.E.Sc

EDUCATION

2010-2012 M.E.Sc Candidate (Biomedical Engineering)
Western University, London, Canada
Characterizing Mechanical Properties of Electrospun
Nanofibers for Tissue Engineering Scaffolds
Supervisor: Dr. Wankei Wan

2006-2010 B.A.Sc, Mechanical Engineering, 2010
University of Toronto (UofT), Toronto, Canada

POSITIONS

2009 **Institute of Biomaterials & Biomedical Engineering at UofT**
Research Assistant, Department of Biomaterials
A Novel Fabrication of Ceramic Bone Implants using Tape Casting
Supervisor: Dr. Robert Pilliar

HONOURS & AWARDS

2011 **Recipient of 3rd place award in Graduate Student Poster Competition**
61st Canadian Chemical Engineering Conference, London, ON, Canada

2010 **Dean's Honours Student**
University of Toronto, Toronto, Canada

2007 **Millennium Bursary - Canada Millennium Scholarship Foundation**
$3000 for the 2007-2008 academic year

2006 **Faculty of Applied Science and Engineering Admission Scholarship**
University of Toronto, Toronto, Canada

2006 **Admission Scholarship from Mechanical Engineering Department**
University of Toronto, Toronto, Canada

2006 **Certificate of Merit for superior achievement in the national
math league contest**

JOURNAL PAPERS (ACCEPTED)

S. Chehreh Chelgani, **S. Makaremi**. Explaining the relationship between common coal analyses
and Afghan coal parameters using statistical modelling methods.
Fuel Processing Technology. 2012.

PUBLISHED CONFRENCE PROCEEDINGS

S. Makaremi, Y. Li, W. Wan. Nanomechanics of Electrospun Poly(Caprolcatone) Nanofibres. Proceedings of the 3rd International Conference on Nanotechnology: Fundamentals and Applications. Montreal, Canada, 2012

R. Rizvi, **S. Makaremi**, S. Botelho, H. Naguib. Piezoresistance Characterization of PDMS-Multiwall Carbon Nanotube Composites. Proceedings of the American Society of Mechanical Engineers (ASME), Philadelphia, USA. 2010

RESEARCH PRESENTATIONS (TALKS)

2012   The 3rd International Conference on Nanotechnology – Montreal, Canada
S. Makaremi, Y. Li, W. Wan. "Nanomechanics of Electrospun Poly(Caprolcatone) Nanofibres"

2012   24th Canadian Materials Science Conference – Western University, London, ON
S. Makaremi, Y. Li, W. Wan. "Mechanical Characterization of Solid and Core-Shell ElectrospunPolycaprolactone (PCL) Nanofibres using Atomic Force Microscopy"

2012   The 25th Annual Western Research Forum – Western University, London, ON, Canada
S. Makaremi, W. Wan. "Electrospun Nanofibres for Tissue Engineering of the Eardrum"

2012   Biomedical Engineering Seminar – Western University, London, ON, Canada
S. Makaremi, J.Hutter, W. Wan. "Nanomechanical Characterization of Electrospun Nanofibres for Tissue Engineering of the Tympanic Membrane"

2011   Nano Ontario Conference and Workshop – McMaster University, ON, Canada
S. Makaremi, N. Sharma and W. Wan. "Mechanical Characterization of Electrospun Polycaprolactone (PCL) Nanofibres using Atomic Force Microscopy"

2011   The 61st Canadian Chemical Engineering Conference – London, ON, Canada
S. Makaremi, J.Hutter W. Wan. "Mechanical Properties of Electrospun Polycaprolactone (PCL) Nanofibres"

2011   Biomedical Engineering Seminar – Western University – London, ON, Canada
S. Makaremi, W. Wan. "Electrospun Nanofibre Scaffolds for Tissue Engineering Tympanic Membrane"

RESEARCH PRESENTATIONS (POSTERS)

2012   London Health Research Day – London, ON, Canada
S. Makaremi, W. Wan. "**Electrospun Nanofibre Scaffolds for Tissue Engineering of Tympanic Membrane**"

2011   **The 61ˢᵗ Canadian Chemical Engineering Conference – London, ON, Canada**
S.Makaremi,J.Hutter, W. Wan. "Mechanical Properties of Electrospun Polycaprolactone (PCL) Nanofibres"

2011   **Margaret Moffat Research Day - Schulich School of Medicine and Dentistry Western University, London, ON, Canada**
S. Makaremi, D.P. Small, W. Wan. "Developing Tissue-Engineered Tympanic Membrane Using Electrospinned Nano-Fibre Scaffold"

TEACHING EXPERIENCE

2012   **Teaching Assistant (Graduate Course)**
Western University – London, ON
Department of Chemical and Biochemical Engineering
Biomaterials, Course Coordinator: Professor W. Wan

2011   **Teaching Assistant (Undergraduate Courses)**
Western University – London, ON
Faculty of Engineering- First Year Common Course
Engineering Design and Innovation Studio,
Course Coordinator: Dr. M. Naish

Western University – London, ON
Department of Chemical and Biochemical Engineering
Tissue Engineering, Course Coordinator: Dr. K. Mequanint

RESEARCH EXPERIENCE

2010-   **Biomedical Engineering Department, Western University Ontario**
MESc Candidate, Characterizing Mechanical Properties of Eletrospun Nanofibres for Tissue Engineering Applications
Supervisor: Dr. Wankei Wan

2009-2010   **Department of Mechanical & Industrial Engineering at UofT**
Undergraduate Thesis, Development of a Novel Electroactive Polymer Sensor for Physiological Monitoring
Supervisor: Dr. Hani. Naguib

2009   **Institute of Biomaterials & Biomedical Engineering at UofT**
Research Assistant, Department of Biomaterials
A Novel Fabrication of Ceramic Bone Implants using Tape Casting
Supervisor: Dr. Robert Pilliar

2009   **Institute of Biomaterials & Biomedical Engineering at UofT**
Summer Student, Department of Biomaterials
Optimization and Trouble Shooting of Grinding Equipment
Supervisor: Dr. Scott Ramsay

2008   **Department of Mechanical & Industrial Engineering at UofT**
        Summer Student**,** Cost Analysis of Manufacturing
        Solid Oxide Fuel Cells
        Supervisor: Prof. Olivera Kesler

2007   **Department of Mechanical & Industrial Engineering at UofT**
        Summer Student, Computer Modelling of Sprays and
        Atomization of Jet Fuel
        Supervisor: Dr. Nasser Ashgriz

TECHNICAL SKILLS

Application Software: Proficient in Solidworks, IGOR Pro, MATLAB, SPSS
         Familiar with Pspice, CosmosWorks

Programming languages: C/C++